

Washington University in St. Louis

Washington University Open Scholarship

All Computer Science and Engineering
Research

Computer Science and Engineering

Report Number: WUCSE-2005-38

2005-08-01

Harmonic Imaging Using a Mechanical Sector, B-MODE

Danna Gurari

An ultrasound imaging system includes transmitting ultrasound waves into a human body, collecting the reflections, manipulating the reflections, and then displaying them on computer screen as a grayscale image. The standard approach for ultrasound imaging is to use the fundamental frequency from the reflected signal to form images. However, it has been shown that images generated using the harmonic content have improved resolution as well as reduced noise, resulting in clearer images. Although harmonic imaging has been shown to return improved images, this has never been shown with a B-mode, mechanical sector ultrasound system. In this thesis, we demonstrated... [Read complete abstract on page 2.](#)

Follow this and additional works at: https://openscholarship.wustl.edu/cse_research

Recommended Citation

Gurari, Danna, "Harmonic Imaging Using a Mechanical Sector, B-MODE" Report Number: WUCSE-2005-38 (2005). *All Computer Science and Engineering Research*.
https://openscholarship.wustl.edu/cse_research/955

Department of Computer Science & Engineering - Washington University in St. Louis
Campus Box 1045 - St. Louis, MO - 63130 - ph: (314) 935-6160.

Harmonic Imaging Using a Mechanical Sector, B-MODE

Danna Gurari

Complete Abstract:

An ultrasound imaging system includes transmitting ultrasound waves into a human body, collecting the reflections, manipulating the reflections, and then displaying them on computer screen as a grayscale image. The standard approach for ultrasound imaging is to use the fundamental frequency from the reflected signal to form images. However, it has been shown that images generated using the harmonic content have improved resolution as well as reduced noise, resulting in clearer images. Although harmonic imaging has been shown to return improved images, this has never been shown with a B-mode, mechanical sector ultrasound system. In this thesis, we demonstrated such a system. First there is a discussion of the theory of harmonic imaging, then a description of the ultrasound system used, and finally experimental results.

Short Title: Harmonic Imaging

Gurari, M.Sc. 2005

WASHINGTON UNIVERSITY
THE HENRY EDWIN SEVER GRADUATE SCHOOL
DEPARTMENT OF COMPUTER SCIENCE AND ENGINEERING

HARMONIC IMAGING USING A MECHANICAL SECTOR, B-MODE
ULTRASOUND SYSTEM

by

Danna Gurari

Prepared under the direction of Dr. William D. Richard

A thesis presented to the Henry Edwin Sever Graduate School of
Washington University in partial fulfillment
of the requirements for the degree of

MASTER OF SCIENCE

August 2005

Saint Louis, Missouri

WASHINGTON UNIVERSITY
THE HENRY EDWIN SEVER GRADUATE SCHOOL
DEPARTMENT OF COMPUTER SCIENCE AND ENGINEERING

ABSTRACT

HARMONIC IMAGING USING A MECHANICAL SECTOR, B-MODE
ULTRASOUND SYSTEM

by
Danna Gurari

ADVISOR: Dr. William D. Richard

August 2005
Saint Louis Missouri

An ultrasound imaging system includes transmitting ultrasound waves into a human body, collecting the reflections, manipulating the reflections, and then displaying them on computer screen as a grayscale image. The standard approach for ultrasound imaging is to use the fundamental frequency from the reflected signal to form images. However, it has been shown that images generated using the harmonic content have improved resolution as well as reduced noise, resulting in clearer images. Although harmonic imaging has been shown to return improved images, this has never been shown with a B-mode, mechanical sector ultrasound system. In this thesis, we demonstrated such a system. First there is a discussion of the theory of harmonic imaging, then a description of the ultrasound system used, and finally experimental results.

to my parents, Shaula and Eitan Gurari

Contents

| | |
|--|----------|
| List of Tables | v |
| List of Figures | vi |
| Acknowledgments | ix |
| 1 Introduction | 1 |
| 1.1 General Problem | 1 |
| 1.2 Overview of Report | 2 |
| 2 Theory of Ultrasound | 3 |
| 2.1 Generation and Detection of Ultrasound Waves | 3 |
| 2.1.1 Piezoelectric Effect | 4 |
| 2.1.2 Piezoelectric Materials | 5 |
| 2.1.3 Ultrasound Wave Generation and Detection | 5 |
| 2.2 Ultrasound Waves on a Particle Level | 6 |
| 2.3 Ultrasound Waves on a Cellular Level | 7 |
| 2.4 Properties of Sound Waves | 8 |
| 2.4.1 Speed | 9 |
| 2.4.2 Frequency | 10 |
| 2.4.3 Reflection | 10 |
| 2.4.4 Attenuation | 11 |
| 2.5 Theory of Harmonic Generation | 11 |
| 2.5.1 Variation of Wave Speed in a Wave | 12 |
| 2.5.2 Amount of Wave Distortion | 14 |
| 2.5.3 Sound Wave Attenuation | 16 |
| 2.5.4 Goldberg's Number | 16 |

| | | |
|----------|---|-----------|
| 3 | Harmonic Imaging | 18 |
| 3.1 | Research That Lead To Harmonic Imaging | 18 |
| 3.2 | Benefits of Harmonic Imaging | 19 |
| 3.3 | Ideal Conditions for Harmonic Imaging | 21 |
| 4 | Ultrasound System | 22 |
| 4.1 | Data Sampling | 23 |
| 4.2 | Data Trimming and Hanning Window | 24 |
| 4.3 | Filtering the Data for Harmonic Frequencies in Software | 27 |
| 4.3.1 | High-Pass Filter | 27 |
| 4.3.2 | Pulse Inversion | 28 |
| 5 | Image Display | 30 |
| 5.1 | Rectification | 31 |
| 5.2 | Envelope Detection | 32 |
| 5.2.1 | Averaging Envelope Detector | 34 |
| 5.2.2 | Optimized Envelope Detector | 35 |
| 5.3 | Scan Conversion | 38 |
| 5.3.1 | Image Display | 41 |
| 6 | Results | 42 |
| 6.1 | Comparison of Envelope Detectors | 42 |
| 6.2 | Fundamental vs. Harmonic Images | 45 |
| 6.3 | Future Work | 47 |
| 7 | Conclusions | 50 |
| | Appendix A Fourier Transform | 51 |
| | Appendix B DFT Leakage and Windowing Functions | 54 |
| | References | 57 |
| | Vita | 59 |

List of Tables

| | | |
|-----|--|----|
| 2.1 | Speed of sound in different media [7] | 9 |
| 2.2 | Factors Determining Phase Speed for a Sound Wave | 13 |
| 2.3 | Media and their B/A values | 14 |
| 2.4 | σ values and their meanings | 16 |
| 2.5 | Attenuation coefficients for some biological media | 16 |

List of Figures

| | | |
|------|---|----|
| 2.1 | Particles in a dense material | 3 |
| 2.2 | Particles in a less dense material | 3 |
| 2.3 | After a mechanical stress is applied to piezoelectric materials, opposite charges line the opposite sides of the material | 4 |
| 2.4 | Axis of non-symmetry on a circular transducer | 5 |
| 2.5 | Particle interaction head on | 6 |
| 2.6 | Particle interaction at an angle (causes beam spread) | 6 |
| 2.7 | Particles in a dense material | 7 |
| 2.8 | Particles in a less dense material | 7 |
| 2.9 | Particles in a less dense material | 7 |
| 2.10 | Effect of low energy pulse on particle | 7 |
| 2.11 | Effect of high energy pulse on particle | 7 |
| 2.12 | Compressions and rarefactions in a sound wave | 8 |
| 2.13 | Detector recording and displaying the signal of a sound wave | 10 |
| 2.14 | Physical change of the shape of a sound wave as it propagates through a medium | 12 |
| 3.1 | Propagating sound beam showing regions of beam spread [15] | 20 |
| 4.1 | Overview of the ultrasound system | 22 |
| 4.2 | Single sine wave pulse | 23 |
| 4.3 | The transducer is shown at five time frames during the data collection process. The black point represents the pivot point of the transducer. | 24 |
| 4.4 | The 256 vectors of data over a 90 degree sweep | 24 |
| 4.5 | A vector of data prior to signal processing | 25 |
| 4.6 | A Hanning window | 26 |
| 4.7 | A vector of data after the Hanning window is applied | 26 |

| | | |
|------|--|----|
| 4.8 | Overlap of fundamental and first harmonic | 28 |
| 4.9 | Wave form of an acoustic pulse emitted by the probe | 29 |
| 4.10 | Wave form of an acoustic pulse 180 degrees out of phase from the pulse shown in figure 4.9 | 29 |
| 5.1 | A 2048 x 256 collection of data | 30 |
| 5.2 | The first image shows five periods of a sine wave and the second image shows the signal after rectification | 31 |
| 5.3 | The first image shows the DFT for five periods of a sine wave and the second image shows the DFT for the five periods of a sine wave after rectification | 32 |
| 5.4 | Original RF signal | 33 |
| 5.5 | Rectified signal | 33 |
| 5.6 | Dotted line shows the desired effects of envelope detection on the rec- tified signal | 33 |
| 5.7 | Ultrasound data | 33 |
| 5.8 | Averaging filter in spatial domain | 34 |
| 5.9 | Magnitude of the DFT of the averaging filter | 35 |
| 5.10 | First image shows the sinc function and the second image shows the hanning window | 36 |
| 5.11 | First image shows the harmonic enveloping detector the second image shows the DFT of the signal | 37 |
| 5.12 | First image shows the fundamental enveloping detector the second im- age shows the DFT of the signal | 37 |
| 5.13 | A 512 x 512 matrix of pixel values used to display the ultrasound data | 39 |
| 5.14 | A 512 x 512 image where the white portion denotes areas where sample data is inserted | 39 |
| 5.15 | Overlap of the vectors from collected data introduces a challenge in determining what value should be displayed at a pixel location | 40 |
| 5.16 | A pictorial example showing the method used to select a vector for sampling | 40 |
| 6.1 | Two fundamental images: the first utilized an averaging envelope de- tector and the second utilized an optimized envelope detector | 43 |
| 6.2 | Pulse inversion harmonic images: the first utilized an averaging enve- lope detector and the second utilized an optimized envelope detector . | 44 |

| | | |
|-----|--|----|
| 6.3 | Fundamental and harmonic images of a cyst | 45 |
| 6.4 | Fundamental and harmonic images of tissue-mimicking substance . . | 46 |
| 6.5 | First plot shows an image obtained where an ideal filter is applied to the data and the second plot shows an image obtained where a Butterworth filter of order 8 is applied to the data | 48 |
| 6.6 | First plot shows an ideal filter and the second plot shows a Butterworth filter of order 8 | 49 |
| B.1 | A continuous periodic signal | 54 |
| B.2 | Sampling exactly 2 samples of the continuous periodic signal and repli- cating this sampled signal into a periodic signal | 54 |
| B.3 | Sampling a non-integer amount of periodic sample and replicating this sampled signal into a periodic signal. Discontinuities arise | 55 |
| B.4 | Rectangular window | 55 |
| B.5 | An example of a frequency domain for a windowing function | 56 |

Acknowledgments

Without Dr. William D. Richard, this thesis could never have been created, so my first thanks are extended to him. In my eyes, he was a fountain of knowledge and it was truly a pleasure to be able to perform research under him and to have him as my advisor. I would like to also thank Dr. Robert Pless and Dr. Roger Chamberlain for serving on my committee. Additionally, I would like to thank Professor David Zar for helping me sort through conceptual holes I had with my research.

Thank you to Tommy Lowery who has been with me through the entire time that I have been working on this thesis. His genuine enthusiasm and eagerness to hear more about my research has helped me take more pride in my work. A thank you is also extended to the many friends who have supported me throughout college, including Maxim Gakh, Emily Hathaway, Pamela Lee, and Rachel Loftspring. Each of their friendships have helped me be that much stronger and accomplish that much more.

My next thanks are extended to my older siblings Inbal, Itai, and Erez who have served as role models throughout my life. Also, thank you to my twin sister, Netta, for her unconditional support and friendship. Finally, I would like to thank my parents, Shaula and Eitan Gurari. Growing up in a home where I saw my father do his research day in and day out and I watched my mother pull 60 to 70 hour work weeks, and seeing them do this while still taking care of five children is the greatest inspiration a person can have. They truly have taught me through example. They have given me the opportunity and the inspiration to achieve all that I have achieved today, and it is to them that this thesis is dedicated.

Danna Gurari

*Washington University in Saint Louis
August 2005*

Chapter 1

Introduction

Ultrasound imaging extends a part of superman's super-powers to the average individual: the ability to view beyond the surface of the skin. This power is accomplished by transmitting ultrasound waves into human body, collecting the reflections, and then using the reflections to generate a grayscale image of the body.

1.1 General Problem

An ongoing problem in ultrasound is that undesired signals are contained in the reflected data. Signals that corrupt the data include:

- Thermal noise generated by the transducer and receiver electronics.
- Reverberations of the ultrasound wave itself.
- Grating lobes which are sound waves that get transmitted from the transducer at angles other than that of the ultrasound wave.
- Scattered and reflected waves resulting from interactions with the many smaller structures throughout tissue.

Consequently, images may show features that are inconsistent with reality.

The standard approach for ultrasound imaging is to use the fundamental frequency from the reflected signal to form images. However, it has been shown through “the triumph of serendipity” that images generated using the harmonic content from reflections have improved resolution as well as reduced noise, resulting in clearer images[2].

The choice to use harmonic imaging to image tissue began as a result of recent experimentation in which it was unexpectedly seen that harmonics are generated when ultrasound waves travel through tissue.

The goal of the research presented in this thesis is to lay the foundation for a mechanical sector B-mode harmonic imaging system. The ultrasound system utilized was designed by Dr. William D. Richard. Then, under his guidance, I assisted Dr. Richard with building the system in the ultrasound laboratory at Washington University.

1.2 Overview of Report

In this thesis, there is first a discussion of the physical properties of sound waves in Chapter 2. Then, in Chapter 3 there is a discussion about why harmonic generation occurs as well as about current research that utilizes harmonic data. Next, there is a description in Chapter 4 about the system used to collect the ultrasound data for both fundamental and harmonic images. In Chapter 5, the techniques for displaying the data are discussed. Finally, the experimental results are shown in Chapter 6.

Chapter 2

Theory of Ultrasound

It is not the goal of this section to predict the amount of harmonic generation that will occur in a particular tissue, but rather to explain the phenomenon essential to this research. With this said, a sound wave can be thought of as a burst of acoustic energy that passes through a medium. In an ultrasound system, the burst of mechanical energy originates at a transducer head and then propagates through the medium as a longitudinal wave [17]. In the following discussion, a medium can be imagined as a large collection of particles where each is bound to all of its neighbors (Figures 2-1, 2-2).

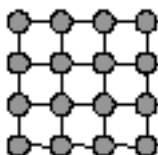


Figure 2.1: Particles in a dense material

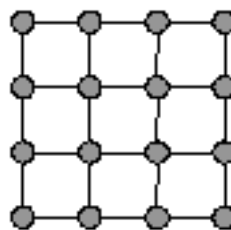


Figure 2.2: Particles in a less dense material

2.1 Generation and Detection of Ultrasound Waves

In ultrasonic imaging, there must be a way to both generate and detect ultrasound waves. Historically, ultrasound sound waves were generated using whistles, sirens, and tuning forks. With these techniques, the upper limit of the frequencies that could be generated was approximately 40 kHz [4]. As for ultrasound wave detection, it

consisted of observing how a cat responds (cats can hear higher sound wave frequencies than humans) or watching the response of a flame after an ultrasound wave was emitted [4].

2.1.1 Piezoelectric Effect

In the 1880s, the Curie brothers and Lippmann both made realizations that are the basis for the current methods of ultrasound wave generation and detection. The Curie brothers discovered that when a mechanical stress is applied to certain materials, an internal electric field is generated such that opposite charges line the opposite sides of the material [4] (Figure 2.3).

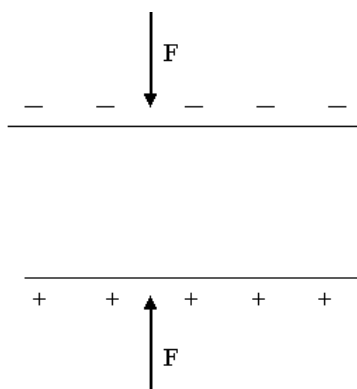


Figure 2.3: After a mechanical stress is applied to piezoelectric materials, opposite charges line the opposite sides of the material

A year later Lippmann predicted that applying an electric field to these materials would cause the material to deform. Shortly afterwards, the Currie brothers proved Lippmann's prediction experimentally [4].

These realizations are the basis for the present day use of piezoelectric transducers in ultrasonic imaging. A transducer is, by definition, a device that converts one form of energy into another [11]. A piezoelectric transducer is a material that converts an electric field into a mechanical stress and vice versa. In contrast to the older tools that generated ultrasound waves with frequencies as high as 40 kHz, piezoelectric transducers allow for ultrasound waves in the 100s of MHz to be generated. Furthermore, the precision of detection available by measuring the voltages in the transducer that

result from the ultrasound wave reflections is much greater than relying on animals and flames for ultrasound wave detection.

2.1.2 Piezoelectric Materials

Materials that exhibit this piezoelectric behavior include the following crystals: quartz, lead zirconate, barium titanate, and lithium niobate [11]. Typically, a slice of the material is taken so that the parallel portions of the element lie normal to an axis of non-symmetry (Figure 2.4).

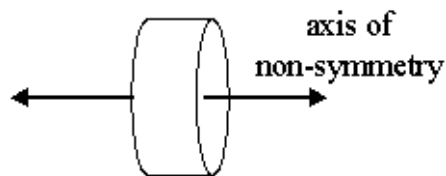


Figure 2.4: Axis of non-symmetry on a circular transducer

The cut is crucial, because a wrong cut can result in suppression of the piezoelectric activity. Furthermore, in order to obtain the piezoelectric behavior, the mechanical stress must be applied to the non-symmetrical axis. In general, ultrasound waves are then generated and detected by placing the piezoelectric element between two plates that can generate and measure an electric field [4].

2.1.3 Ultrasound Wave Generation and Detection

Before and after any electrical or mechanical force is applied to a piezoelectric element, the charge of the material is neutral. In other words, there is no voltage across the crystal. For generation of an ultrasound wave, an electric voltage is applied to the material. The polarity of the voltage that reaches the material determines the type of mechanical response of the element. The element either becomes thinner and longer or shorter and fatter than the material was at rest. Since the change in shape depends on the polarity of the voltage, the shape of the ultrasound wave can be controlled by controlling the voltage across the piezoelectric element.

Detection of ultrasound waves is the reverse procedure of ultrasound wave generation. The polarity of the voltage across the piezoelectric element is determined by whether

the piezoelectric material is pushed (made thinner and longer) or pulled (made shorter and fatter) by the reflection of the ultrasound wave.

In summary, a piezoelectric transducer is used for both ultrasound wave generation and detection. Initially, to generate ultrasound waves, the piezoelectric element converts an applied voltage to mechanical ultrasound waves. Then, as the reflections of the sound waves arrive to the transducer face, it converts that mechanical energy back into electrical energy.

2.2 Ultrasound Waves on a Particle Level

One way to describe the sound wave produced by the transducer is to explain the response of each of the particles in the medium to a sound wave. In this description, a sound wave is defined as the domino effect of one particle hitting the next particle which, in turn, hits the next, and so on. Note that particles are not always directly aligned and so, at times, particle-particle interactions cause energy to be passed at angles (for ultrasound, this means that beam spread is occurring) (Figures 2.5, 2.6).



Figure 2.5: Particle interaction head on

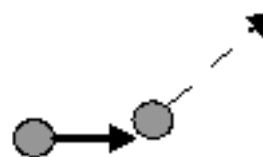


Figure 2.6: Particle interaction at an angle (causes beam spread)

The impact from the collision of two particles can be represented mathematically as the balance between two forces acting on a mass. The amount of force initially acting upon each particle (the energy imparted to it) is given by Newton's Second Law which states that force is a function of the particle's mass and acceleration ($F = ma$) [17]. In the case that several particles hit a particle simultaneously, the striking energy is the combined effect of all the striking particles. After a particle is struck and displaced from equilibrium, a force acts in opposition returning the particle to its equilibrium. Hooke's Law, which assumes linear interactions, treats the particle as a mass on a spring and says that the restoring force is proportional to the length the spring is stretched ($F = -kx$) [17]. Typically, the restoring force causes so much inertia to the particles that they overshoot and pass their equilibrium. Consequently, after particles

are struck, they tend to vibrate around equilibrium [17]. The balance between these two forces around equilibrium is shown below in Figures 2.7, 2.8, and 2.9.

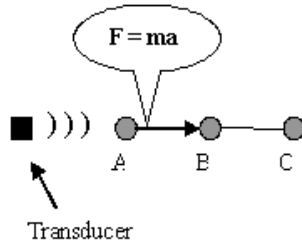


Figure 2.7: Particles in a dense material

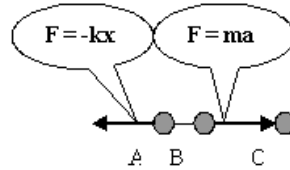


Figure 2.8: Particles in a less dense material

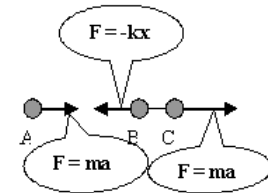


Figure 2.9: Particles in a less dense material

Since $ma = -kx$ and since k is a constant, if a particle is struck with a greater force ($F = ma$), the particle will respond by traveling a larger distance, x . In other words, force determines the distance the particle travels from its resting position; a greater force means greater particle displacement. So for ultrasound, if a high energy (large amplitude) sound beam is transmitted through a medium, then the particles in the propagation path are displaced from their rest position more than if a low energy beam is transmitted through a medium (Figures 2.10, 2.11).

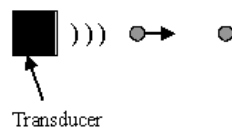


Figure 2.10: Effect of low energy pulse on particle

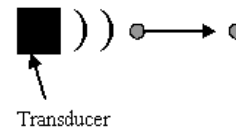


Figure 2.11: Effect of high energy pulse on particle

In summary, at the particle level, a single sound wave is the passing of energy from particle to particle from one side of a medium to the other. Furthermore, increased energy means greater particle displacement.

2.3 Ultrasound Waves on a Cellular Level

A second model describes sound wave behavior at the cellular level focusing on the cumulative effects from each of the particle-particle interactions. In this model, sound waves can be described as compressions and rarefactions traversing through a medium.

Zooming in to the individual particle interactions, when one particle hits the second, the two particles are pushed together. As a result, a higher pressure region (compression) is generated. Then, when that first particle bounces backwards and the second particle is flung forward, the two particles are pulled apart. In other words, a lower pressure region (rarefaction) is created [11]. Zooming back to a cellular view of a propagating sound wave, as a wave passes through a medium, most particles respond similarly to the sound wave resulting in areas in the medium where the net sum of the particles in the region are either simultaneously pulled apart or pushed together; in other words, there are compressions and rarefactions (Figure 2.12).

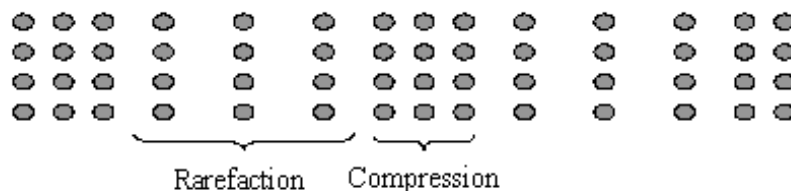


Figure 2.12: Compressions and rarefactions in a sound wave

A higher energy sound beam causes individual particles to travel further from their rest position than a lower energy sound beam. Consequently, the net effect of many particles displacing simultaneously from a higher energy sound beam results in regions of the medium with drastically higher and lower densities than would arise if a lower energy sound beam passed through the medium.

In summary, at the cellular view, sound waves are viewed as rarefactions and compressions propagating through a medium. Additionally, a higher energy sound wave causes more drastic changes to the density of a medium than a low energy sound wave.

2.4 Properties of Sound Waves

Several sound wave properties key to understanding the focus of this research are the following: speed, frequency, reflection, and attenuation. For this section, discussion of sound waves refers to sound waves on the cellular level.

2.4.1 Speed

Speed is defined as the distance one compression or rarefaction in a sound wave travels in the medium in a unit of time, and is determined with the following equation:

$$v = w \times f \quad (2.1)$$

where v is the speed of sound, w is the wavelength of the sound wave, and f is the frequency of the sound wave [17]. The speed of a sound wave is determined by the propagating medium. While media of varying properties propagate sound at different speeds, the wave's speed in a single medium remains constant as long as the temperature and the properties of the medium are held constant [17]. Table 2-1 shows approximations for the speed of sound in seven materials.

Table 2.1: Speed of sound in different media [7]

| Medium | Speed of Sound (meters/second) |
|--------------|--------------------------------|
| Air | 330 |
| Fat | 1,450 |
| Water | 1,480 |
| Human Tissue | 1,540 |
| Kidney | 1,561 |
| Muscle | 1,585 |
| Skull Bone | 4,080 |

Mainly two properties of a medium are considered to affect sound wave speed: elasticity and inertia of the particles within the propagating medium [19]. The first property, elasticity, is defined as the degree to which a medium resists deformation when a force is applied to it. Typically, solids have higher elasticity than liquids which in turn have higher elasticity than gases. Furthermore, sound waves tend to propagate faster in media with higher elasticity. The second property, inertia, determines the responsiveness of individual particles to their neighboring particles. A greater inertia indicates a medium is composed of particles with larger mass-densities. Sound waves propagate faster in media with less particle inertia. The following equation shows the relationship between sound wave speed and these two properties of a medium [19]:

$$v = \sqrt{\frac{E}{\rho}} \quad (2.2)$$

where E is Young's modulus of elasticity, ρ is the material density, and v is the speed of sound.

2.4.2 Frequency

Frequency is defined as the number of wave lengths passing through a point per second. In ultrasound, the frequency of a sound wave can be discerned by counting how many times per unit of time either a high pressure (compression) or a low pressure (rarefaction) passes a particular location. A detector can be used to record the pressure variations propagating through the medium (Figure 2.13).

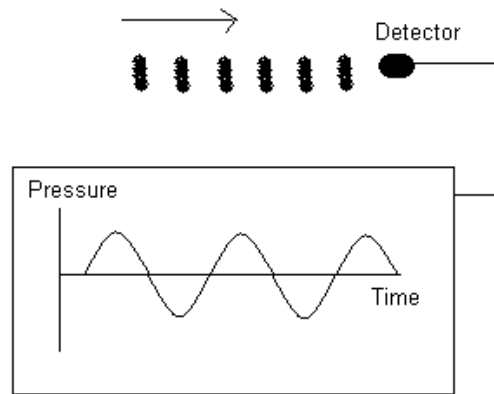


Figure 2.13: Detector recording and displaying the signal of a sound wave

When the frequency of the sound wave is not obvious from the recorded signal, a Fourier Transform can be performed on the signal in order to determine the frequencies of which the sound wave is comprised as well as the proportions of the sound wave that are at each of these frequencies [17].

2.4.3 Reflection

When a sound wave encounters the end of one medium and the beginning of another one (a boundary), a portion of the transmitted energy gets reflected. The equation used to determine the amount of energy that gets reflected is as follows [17]:

$$R = \left(\frac{Z_2 - Z_1}{Z_2 + Z_1} \right)^2 \quad (2.3)$$

where Z_1 is the acoustic impedance of the first medium, Z_2 is the acoustic impedance of the second medium, and R is the fraction of the energy that gets reflected. Clearly, this equation depends on the acoustic impedances of the two media. Therefore, measuring these acoustic impedances is necessary to evaluate the amount of reflection. The equation for finding acoustic impedance is as follows [17]:

$$Z = p \times v \quad (2.4)$$

where Z is the acoustic impedance of a material, p is the density of the material, and v is the speed that sound travels in the material. From the mathematical equation for finding a reflection, it can be concluded that a greater difference in acoustic impedances between two neighboring media results in a greater amount of reflection. Note that any energy that is reflected at a boundary is lost from the energy of the propagating sound wave.

2.4.4 Attenuation

Attenuation is the diminishing of the original sound wave's energy resulting from the combined effects of both scattering and absorption [8]. For ultrasonic imaging, attenuation is significant because it determines the depth of wave penetration possible and, thus, the depth of imaging that is possible. Scattering occurs when energy reflects from a very small obstacle and absorption occurs when particles in the path of the ultrasound wave retain some of the energy from the wave, possibly in the form of heat [19]. It follows that sound wave and media characteristics that are more conducive to scattering and absorption dissipate sound waves more quickly. One example is the dependency of the degree of attenuation on the sound wave frequency. Sound waves at a higher frequency tend to have greater amounts of energy absorbed by the media and, consequently, higher frequency sound waves tend to dissipate more quickly than low frequency sound waves within the same media.

2.5 Theory of Harmonic Generation

David T. Blackstock, an expert and leader in the field of non-linear acoustics, summarized the historical development that led to the discovery of harmonic generation. According to his account, it took over 200 years and a foundation of work from such well-known individuals as Euler, Earnshaw, Riemann, Lagrange, Poisson, Stokes,

Airy, Fay, Fubini, and Langevin to discover the non-linear nature of sound waves [8]. From their work, it was eventually determined that sound waves propagate in a non-linear manner and, furthermore, this non-linearity causes harmonic development.

When treating sound waves as having finite amplitudes, the explanation for the non-linear behavior of sound waves is quite simple. Ultrasound waves behave as pressure waves compressing and expanding the medium that they pass through with the compressed regions having increased density and the expanded regions having decreased density. The speed at which a wave propagates through a medium depends partly on the medium's density with waves traveling faster in denser media. Consequently, the compressed regions of a medium propagate sound waves faster, and the expanded regions propagate sound waves slower. As a result, sound waves experience a gradual physical change similar to the one that is shown in Figure 2.14 [8]:

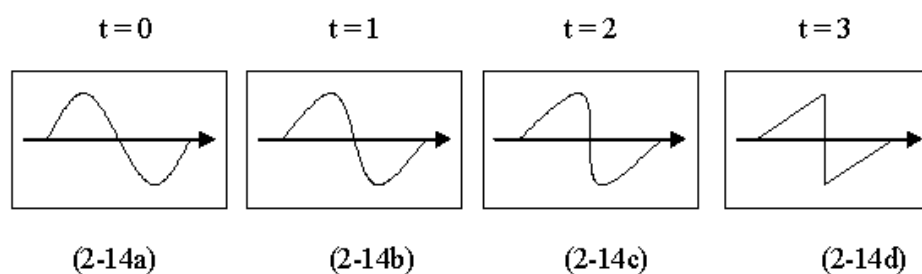


Figure 2.14: Physical change of the shape of a sound wave as it propagates through a medium

A linear propagation of the sound wave would mean that the transmitting wave would propagate in the physical shape shown in figure 2.14a. Thus, the physical change seen in Figures 2.14b-d indicates that there is a growing addition of harmonics to the propagating sound waves.

2.5.1 Variation of Wave Speed in a Wave

From Figure 2.14, it is clear that the wavelength of the sound waves remains constant regardless of the degree of distortion occurring from point to point within the wave form. Thus, assuming a linear sound wave where the frequency of the sound wave remains constant during propagation, it makes sense that the speed of the sound wave should be the value determined by $v = w \times f$; this speed is called c_0 . However, it is clear from Figure 2.14 that the wave speed varies for different phases of the

sound wave and this indicates that there is an addition of harmonics to the sound wave. It was eventually discovered that two non-linear factors contribute to the speed variation within the waveform. First, convection affects individual particle behavior introducing the particle velocity, u , into the phase speed and, second, the relationship between pressure variation and density variation in a medium is nonlinear introducing a speed that depends on the properties of the medium into the phase speed (Table 2-2) [8].

Table 2.2: Factors Determining Phase Speed for a Sound Wave

| Non-linear | Linear |
|---|-----------------------|
| - Convection - Non-linear properties of the medium | - Speed of sound wave |

By superimposing these three factors, one can derive the following mathematical equations for approximating phase speed of a sound wave traveling through liquids and gases [8]:

$$v_t = c_0 + u + \frac{1}{2}(\gamma - 1)u \quad (2.5)$$

$$v_t = c_0 + u + \frac{1}{2}\left(\frac{B}{A}\right)u \quad (2.6)$$

Equation 2.5 is for gases, and equation 2.6 is for liquids. In these equations, v_t is the phase speed of the sound wave, c_0 is the sound speed for a small-signal sound wave, u is the particle velocity, and $(\gamma - 1)$ and $\left(\frac{B}{A}\right)$ are the coefficients for the nonlinearity of a medium [8]. More generally, the equation can be written as follows:

$$v_t = c_0 + \beta u \quad (2.7)$$

where β is the coefficient of nonlinearity and is defined as follows [5]:

$$\beta = \frac{(\gamma + 1)}{2} \quad (2.8)$$

$$\beta = 1 + \frac{B}{2A} \quad (2.9)$$

Equation 2-8 is for liquids and equation 2-9 is for gases. Because a portion of non-linearity depends on the non-linear quality of the medium, it is important to know

the contribution of speed resulting from the non-linearity of the medium ¹. For the purpose of this paper, it is sufficient to say that a significant amount of work has been devoted to determining $\frac{B}{A}$ values for a range of biomedical media. Table 2-3 lists several ² [2].

Table 2.3: Media and their B/A values

| Biomedical Medium | B/A Values |
|---------------------|------------|
| Water | 4.96 |
| Whole Blood | 6.1 |
| Nonfat soft tissues | 6.3-8.0 |
| Fatty soft tissues | 9.6-11.3 |

Although a larger value of $\frac{B}{A}$ indicates that a greater amount of harmonics are generated by a medium, it will be seen that this value is not sufficient in itself to indicate how effective harmonic imaging will be in a particular medium.

2.5.2 Amount of Wave Distortion

Something further that can be seen in Figure 2.14 is that sound wave distortion increases with time. This is because the effects of convection and the non-linearity of the pressure-density relation accumulate with propagation distance. More specifically, the distortion occurring at any location merely adds to any distortion that was already present [5]. The equation below is a computation that allows for the amount of sound wave distortion to be discerned [8]:

$$\sigma = z\beta\epsilon\kappa \quad (2.10)$$

where z is the distance the wave has traveled, β is the coefficient of nonlinearity, ϵ is Mach's number at the source, and κ is the wave number. From the equation above, it follows that the amount of harmonics generated is linearly dependent on the following factors:

¹An in-depth description is given in Hamilton and Blackstocks book, Nonlinear Acoustics, about techniques employed to determine $\frac{B}{A}$ values [8].

²Since the scope of the presented research is focused on imaging biomedical media which are considered to be liquids, the non-linear measurements for gases are ignored. Values for the coefficients of non-linearity for gases can be found in Hamilton and Blackstock's book titled Nonlinear Acoustics [8].

- distance the sound wave travels
- coefficient of non-linearity which depends on the amount of non-linearity in the medium ($\frac{B}{A}$)
- acoustic pressure at source ($\varepsilon = \frac{u_0}{c_0}$ where u_0 is the acoustic pressure at the source and c_0 is the wave speed)
- frequency ($\kappa = \frac{2f\pi}{c_0}$ where f is the frequency).

Therefore, the farther a sound wave travels, the greater the amount of harmonics generated. Furthermore, a medium with a higher $\frac{B}{A}$ value results in richer amounts of harmonics. Since harmonic generation requires that the amplitude of the propagating wave be large enough, a larger acoustic pressure at the source contributes to larger amounts of harmonic generation. Conceptually, this is because greater energy causes much higher and lower density regions in the medium, which in turn results in waves propagating significantly faster and slower leading to greater sound wave distortion. Finally, sound waves of higher frequencies arrive at acoustic shock more quickly. Conceptually, this relationship makes sense too since less of a deformation is required for the waveform to change from its current wave shape to a shock formation.

Values of σ range from 0 to 4 and larger values signify a greater amount of harmonic content. Values below 1 indicate a small amount of harmonic content. However, when σ equals 1 shock formation occurs. Shock generation implies that a part of the propagating sound wave is exactly vertical; this is seen in both Figures 2.14c and 2.14d. When shock formation occurs, the amount of harmonic generation is said to become significant. Values increasing from 1 up to 3 indicate a greater growth in harmonic content; visually, this means that the amount of the wave that is vertical becomes greater. Finally, values from 3 to 4 indicate a sawtooth formation [8]. Figure 2.14d represents the saw-tooth formation³. For this paper, it is sufficient to say that from the moment that the saw-tooth formation occurs, enough dissipation of the sound wave occurs to prevent any further distortion of the sound wave [8]. Table 2-4 summarizes the correlation between values of σ and the degree of harmonic generation.

³An in-depth description is given in Hamilton and Blackstock's book, Nonlinear Acoustics, about saw-tooth formation [8]

Table 2.4: σ values and their meanings

| σ value | 0-1 | 1-3 | 3-4 |
|--|-----|-----|-----|
| Significant Harmonic Content? | No | Yes | Yes |
| Shock Formation? | No | Yes | Yes |
| Sawtooth Formation (Greatest Amount of harmonics)? | No | No | Yes |

2.5.3 Sound Wave Attenuation

Attenuation occurs whenever a sound wave propagates through a medium, and attenuation is represented mathematically by the symbol α . Table 2-5 shows the attenuation coefficients for some biological media [3].

Table 2.5: Attenuation coefficients for some biological media

| Biomedical Medium | Temperature (Celsius) | Frequency (MHz) | Attenuation Coefficient (dB cm ⁻¹) |
|-------------------|-----------------------|-----------------|--|
| Amniotic Fluid | 22 | 2 | 0.045 |
| Blood | 25 | 1 | 0.21 |
| Breast | in-vivo | 1.76 | 0.5-1.1 |
| Skin | 23 | 1 | 3.5 ± 1.2 |

The degree of attenuation depends on the interaction between the sound wave and the medium, or more precisely, the amount of the sound wave energy that is absorbed and scattered. For example, sound waves of a higher frequency are attenuated more than sound waves at a lower frequency, because more energy is absorbed by the media during propagation. A more recent discovery has shown that attenuation is the key player in limiting the amount of harmonics that can be generated in a propagating wave. Theoretically and mathematically, there exists a saturation point for the amount of harmonics that can be generated, and any attempt to add more harmonics to the propagating sound wave is prevented by a corresponding increase in attenuation [8].

2.5.4 Goldberg's Number

In conclusion, the amount of harmonics generated can be viewed as a battle between two forces: harmonic generation arising from the nonlinear nature of sound waves and attenuation. Both of these values can be input into an equation from which the amount of harmonics can be estimated [8]:

$$\Gamma = \frac{l_a}{l_d} \quad (2.11)$$

In this equation, Γ is the Goldberg number, l_a is the absorption length ($\frac{1}{\alpha}$), and l_d is the distance at which a shock first forms in the absence of dissipation ($\frac{1}{\beta\varepsilon\kappa}$). Values of the Goldberg number less than one signify that attenuation effects dominate the propagation of the wave form, equaling one signify that the contributions from the nonlinearity and attenuation are about equal, and exceeding one signify that the nonlinear effects dominate. The third case is desirable for harmonic imaging.

Chapter 3

Harmonic Imaging

In ultrasonic imaging, imaging is done directly from the reflections of a transmitted ultrasound wave. The common assumption is that ultrasound waves behave linearly; in other words, the frequency content of a sound wave remains constant through propagation. It follows then that reflections from the sound wave will only reflect at that propagated frequency. Therefore, only the frequency of the transmitted sound wave should be extracted from the reflected signal and used for imaging. This type of imaging is the standard mode of imaging. However, because sound waves behave non-linearly, it is clear that frequencies other than the transmitted frequency are produced within a propagating sound wave. Thus, reflections from the sound wave at boundaries are also at harmonic frequencies (frequencies that are multiples of the fundamental frequency). Imaging that extracts the harmonic frequencies from a reflected signal and uses those for imaging is called harmonic imaging. Harmonic imaging is advantageous over the standard mode of imaging because images tend to have less noise and higher resolution, and consequently improved image clarity [2].

3.1 Research That Lead To Harmonic Imaging

Although the theory for harmonic imaging has been around since the 1950s, the use of harmonics to image biological tissues did not occur until the 1990s. The development of tissue harmonic imaging resulted from “the triumph of serendipity over logical progression” [2].

Initially, in ultrasound, harmonic imaging was limited to experiments that imaged blood flow with the use of contrast agents (free gas bubbles). It was known that gas

bubbles are highly nonlinear and so, once struck by an ultrasound wave, gas bubbles generate large amounts of harmonics [3]. Consequently, by releasing contrast agents into the bloodstream and then imaging areas for harmonics, areas of blood flow were located.

With time, it became evident that harmonic content was produced within the body in areas without contrast agents albeit to a much lesser degree. As a result, research utilizing harmonic generation was performed without the use of contrast agents. In one research project, ultrasound waves were propagated through the bladder and the amount of generated harmonics was correlated to a distance of liquid through which the wave must have traveled. Using the estimated liquid distance, the bladder volume was then predicted [1]. This research was possible because the surrounding regions of the bladder are made of tissue, and tissue generates insignificant amounts of harmonics relative to liquids due to the greater absorption of energy from the medium.

Although harmonic generation in tissues is relatively insignificant, enough harmonics are generated in the tissue to allow for harmonic imaging. A less technical article titled “Ensemble™ Tissue Harmonic Imaging: The Technology and Clinical Utility” discusses several doctors’ testimonials about using the ultrasound harmonic imaging system SONOLINE Elegra, sold by Siemens Medical. Four doctors describe how diagnoses that were missed through fundamental imaging were able to be made with harmonic imaging and that, in general, diagnoses are more easily made using harmonic images [7].

3.2 Benefits of Harmonic Imaging

An ongoing problem in ultrasonic imaging is that undesired signals are contained in the reflected data. For emphasis, the signals that corrupt the data are reiterated below:

- Thermal noise generated by the transducer and the receiver electronics.
- Reverberations of the ultrasound wave itself.
- Grating lobes which are sound waves that get transmitted from the transducer at angles other than that of the ultrasound wave.

- Scattered and reflected waves resulting from interactions with the many ‘smaller structures throughout tissue.

These signals are mixed with the propagated sound beam. Recall that a sound beam is transmitted from a vibrating piston called a transducer [19]. The piston causes a sound wave at a specified frequency to propagate through the medium. One would expect the emitted sound beam to propagate in the direction at which the energy is imparted to the body (Figure 3-1). However, in actuality, beam spread occurs [14].

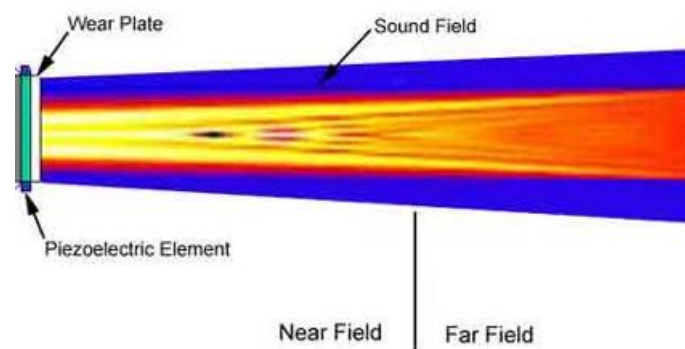


Figure 3.1: Propagating sound beam showing regions of beam spread [15]

The area of the sound beam where the energy content is greatest is within the center of the beam; in other words, the area of the sound beam shown in Figure 3-1 that is lighter in color [5]. Areas external to the center of the sound beam contain significantly less energy. Recall that insignificant amounts of harmonics develop from low energy sound waves, while lots of harmonics generate from high energy sound waves. Consequently, reflections from the central portion of the sound beam contain large amounts of harmonic signal while reflections from other parts of the sound beam contain relatively insignificant amounts of harmonic signal.

Therefore, images derived from the harmonic signal are indicative mainly of the reflections coming from the center of the sound beam. Since a portion of the undesired signal is contained outside of the center of the sound beam, harmonic imaging succeeds in removing some of the signals that corrupt the image. Consequently, fewer artifacts and noise arise in harmonic images. Additionally, because the harmonic content is mainly contained in the central portion of the sound beam, the lateral beam width is narrower. This, in turn, means that there is improved lateral resolution. Also, a

medium reflects energy for the length of time that the waveform passes through a boundary. This means that the less time a waveform passes through a boundary the less amount of time it generates reflections resulting in higher axial resolution. Consequently, since harmonic imaging utilizes higher frequency waves, the images benefit from improved axial resolution.

3.3 Ideal Conditions for Harmonic Imaging

Although harmonic imaging has clear benefits, these benefits are not seen in all imaging environments. As is suggested by theory and supported by experiments, there are significant variations in the amount of harmonics generated in varying media, and the farther a wave travels the greater the amount of harmonic generation. Thus, imaging a region of interest using harmonic imaging requires that it is possible for enough harmonics to be generated by the time the ultrasound wave arrives at the region of interest. This depends largely on the type of media that is being imaged [1]. For instance, in tissue, imaging shallow objects using harmonic imaging returns inferior images to that of fundamental imaging since very few harmonics have been generated in the shallower regions.

Chapter 4

Ultrasound System

Discussion of the ultrasound system will refer to the system shown in Figure 4-1.

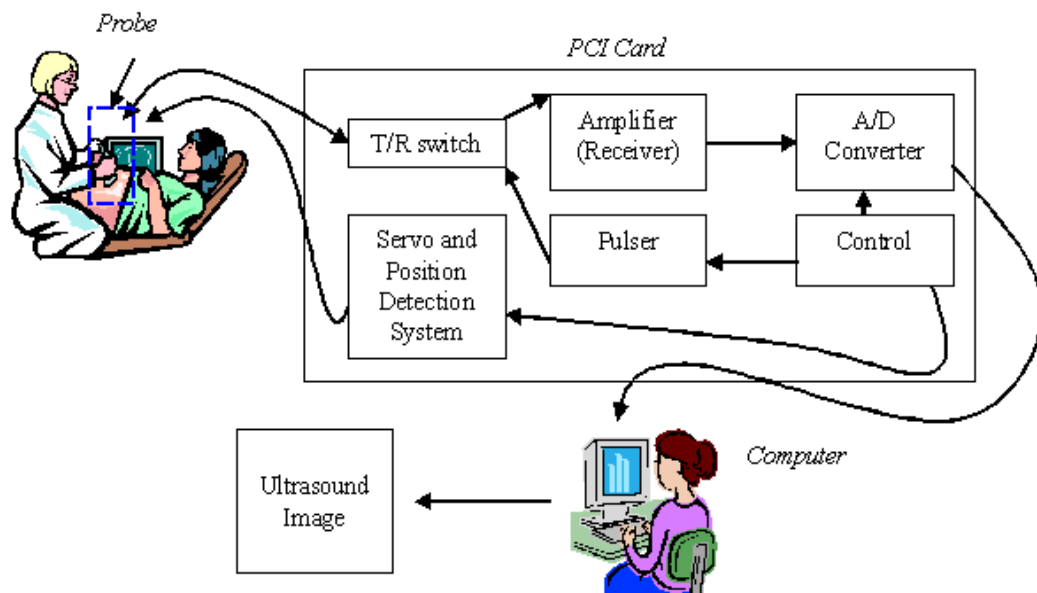


Figure 4.1: Overview of the ultrasound system

This system was designed in the Ultrasound Laboratory at Washington University in St. Louis and consists of a PCI card with a control circuit, pulser, transmitter/receiver (T/R) switch, servo, position detection system, probe, amplifier (receiver), and an A/D converter, and a computer. Gray scale, B-mode images are produced with this system, where a B-mode image is defined to be a 2-D image that is created using a succession of 1-D reflected ultrasound signals [18]. The resulting brightness at each pixel in the 2-D image indicates the amplitude of the reflections with whiter shades

indicating signals with higher amplitudes and blacker shades indicating signals with smaller amplitudes [18]. The focus in this chapter is on how the succession of 1-D reflections is obtained, and the focus in the next chapter is on how a 2-D image is generated from these 1-D reflections.

4.1 Data Sampling

The probe utilized in this research is a GP2000 sold by Interson. The transducer within the probe has a natural frequency of 5 MHz with 100 percent bandwidth. Data collection begins when the pulser on the PCI card sends a pulse of electrical energy to the transducer in the probe. The pulse in this research is a single cycle of a sine wave that can be as large as ± 125 V. Figure 4-2 shows a single cycle of a sine wave with a range of ± 10 V.

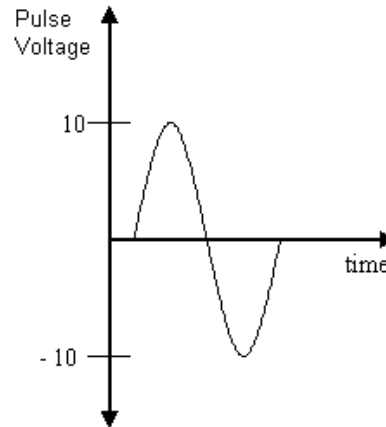


Figure 4.2: Single sine wave pulse

The transducer, because of its piezoelectric nature, transforms this electrical energy into mechanical energy. This energy is then emitted as an ultrasound wave with a center frequency of approximately 3.5 MHz. After emission, the T/R switch causes the electronics to switch to receive mode, and the reflected wave is received as a continuous time signal using the transducer as a piezoelectric microphone¹. As the acoustic energy arrives to the probe, the piezoelectric property of the transducer causes this mechanical energy to transform into an electric voltage, which is then

¹A direct connection between the pulser and amplifier would result in the amplifier being damaged. In order to prevent the passage of the electrical energy from the pulser to the amplifier, a T/R switch is used.

forwarded through a coaxial cable to the receiver on the PCI card. At the receiver, the signal is amplified and then is sampled using an 8-bit A/D converter at a sampling frequency of 50 MHz. After 2048 samples are collected, the T/R switch returns the electronics back to pulse mode and the servo and position detection system cause the transducer within the probe to rotate. This collection of data is repeated until 256 vectors of 2048 sample points each are collected, with the resulting collection of data spanning 90 degrees (Figures 4.3 and 4.4).

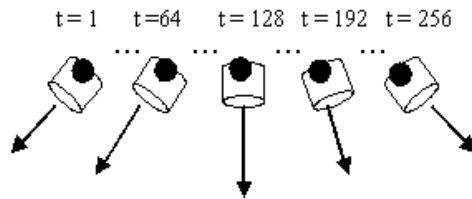


Figure 4.3: The transducer is shown at five time frames during the data collection process. The black point represents the pivot point of the transducer.



Figure 4.4: The 256 vectors of data over a 90 degree sweep

The transducer, during data collection, pivots about a point offset from the transducer face as shown in Figure 4.3. As a result, the first sample values for each of the 256 vectors of data do not all meet at the same point. This is shown in Figure 4.4.

4.2 Data Trimming and Hanning Window

Once the sampling is completed, the data is forwarded from the PCI card to the memory inside the computer. An example of a vector of data that arrives in memory is shown below in figure 4.5.

This data was obtained using the ultrasound system to image a part of a phantom, Gammex RMI 404GS [6].

An undesirable part of this data is the initial portion containing samples with values around ± 100 (approximately the first 400 samples). The data in these reflections arise when the sound wave crosses the probe membrane into the phantom. Since the objective is to image the tissue-mimicking substance within the phantom, it is not necessary to retain the first portion of the data. Additionally, the amplifier

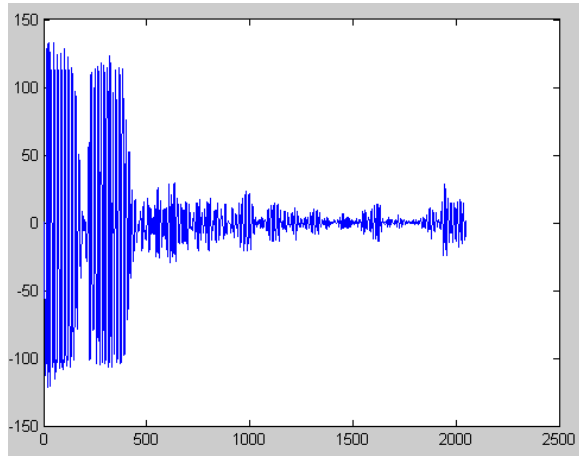


Figure 4.5: A vector of data prior to signal processing

is saturated when receiving this data meaning that the amplification is non-linear. Therefore, removing this initial portion of the signal is desirable to ensure the data is indicative of only the reflections from within the phantom. Consequently, the first 400 sample values are all set to zero.

A windowing function is then applied to the remaining 1648 samples in order to minimize the amount of DFT leakage. Minimizing DFT leakage is an important task in itself; however, for this research, it is even more critical because the higher frequency content is the data used for imaging. If higher frequencies resulting from leakage overwhelm the higher frequency content in the data, the images will be indicative of the information in the artifacts as opposed to the information in the reflected sound wave itself. The windowing function used to minimize DFT leakage is a Hanning window. A description of DFT leakage is given in Appendix B.

The signal multiplied with each vector of reflected data consists of two parts. The first part sets the values in the initial portion of data to zero and the second part multiplies the remaining part of the untouched data with a Hanning window. The coefficients of the Hanning window are derived from the following equation:

$$r[k] = 0.5 \left(1 - \cos \left(2\pi \frac{k}{n-1} \right) \right) \quad (4.1)$$

where r is the vector holding the Hanning window coefficients, k is the index into the vector, and n is the number of samples. More specifically, a vector of 400 values

set to zero was inserted into a vector² and then a 1648 point Hanning window was appended to the vector. Figure 4-6 shows the resulting window:

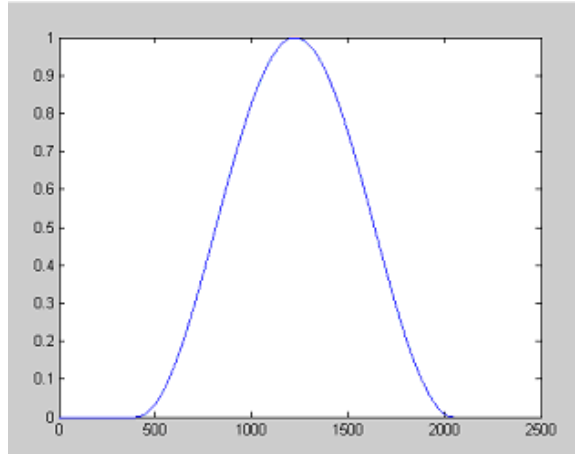


Figure 4.6: A Hanning window

Figure 4-7 shows the effect of multiplying the Hanning window with the signal shown in figure 4-5.

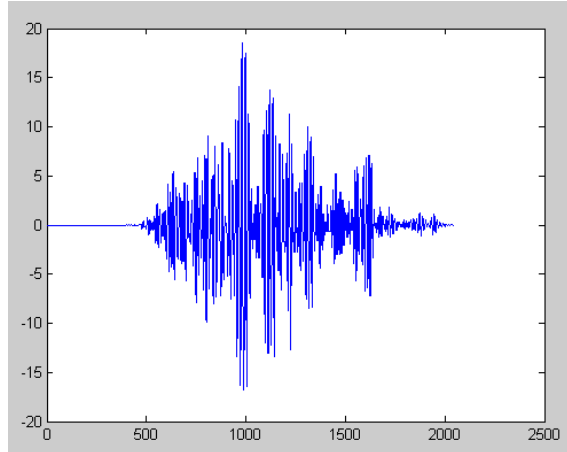


Figure 4.7: A vector of data after the Hanning window is applied

Note, that this windowing function may not be the optimal window. This window preserves the frequency content of the data at the expense of diminishing the intensity of the data in the time domain.

²The number of samples in the initial part of the signal that show saturation was determined, through observation, to be the first 400 samples.

4.3 Filtering the Data for Harmonic Frequencies in Software

The subsequent data processing depends on the type of image that is being generated: fundamental, harmonic using high-pass filtering, or harmonic using pulse inversion. For a fundamental image, the signal is ready for the imaging process. This process is discussed in Chapter 5. For the harmonic images, the signal processing for the two techniques is described below.

4.3.1 High-Pass Filter

Since high-pass filtering requires using a Discrete Fourier Transform (DFT), a brief discussion on the DFT is given in Appendix A. First the signal is passed through a DFT and then a high-pass filter is applied to the transformed signal to remove the frequency components not in the harmonic portion. The resulting filtered signal is then passed through an inverse DFT to return the signal back to the time domain. This resulting signal is used for imaging and goes through the imaging process described in Chapter 5.

The high-pass filter utilized is a Butterworth filter of order 8 with a cut-off frequency that is 1.5 times the fundamental frequency. The coefficients for the Butterworth filter are found using the following equation:

$$H(d) = \frac{1}{1 + \left(\frac{D_0}{d}\right)^{2n}} \quad (4.2)$$

where H is the vector of Butterworth coefficients, d is sample number of the data, D_0 is the cut-off frequency, and n is the order of the filter.

The general form of the magnitude plot of the Fourier Transform for a reflected ultrasound pulse in this ultrasound system is shown in figure 4.8.

Note that the first harmonic has a reduced amplitude; this is due to the greater attenuation that higher frequencies experience during propagation within a medium. Also, the reflected ultrasound waves have a range of frequency information that are centered around the fundamental and harmonic frequencies meaning that other frequencies than simply the fundamental and harmonic frequencies are included in the data. The reason for this non-spike like shape is that, in practice, the frequency

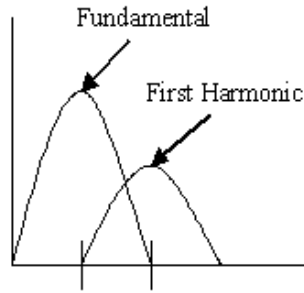


Figure 4.8: Overlap of fundamental and first harmonic

content for the emitted ultrasound waves has this non-spike like form. Consequently, the reflections have this form too. This overlap of the fundamental and harmonic frequencies means that any filtering will, inevitably, cut part of the harmonic signal out while retaining part of the fundamental signal. Therefore, high-pass filtering provides a flawed means for extracting the harmonic signal from the reflected ultrasound data. One way to reduce, or even remove, the overlap would be to alter the shape of the emitted ultrasound energy. For example, by driving a transducer with several cycles of a sine wave, the bandwidth of the transmitted pulse would be narrowed.

4.3.2 Pulse Inversion

The second method, pulse inversion, returns harmonic data which is, in theory, free of the fundamental information. Due to the non-linear nature of harmonic frequencies, adding two echo signals that are generated by transmitting pulses out of phase by 180 degrees causes the linear portions (the fundamental portions) as well as the odd harmonics to zero out while the even harmonics double. Figures 4.9 and 4.10 show the general form of two acoustic waves that are emitted from the probe in order to obtain the two sets of vector data containing linear signals that are out of phase by 180 degrees.

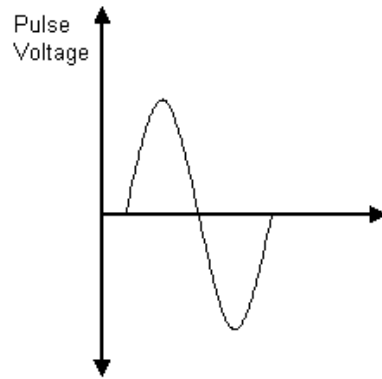


Figure 4.9: Wave form of an acoustic pulse emitted by the probe

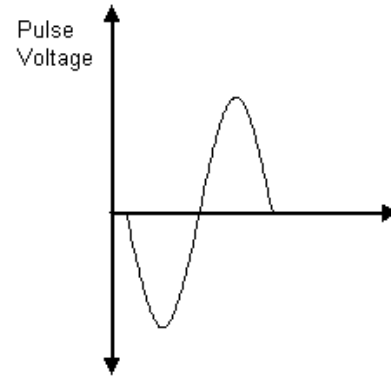


Figure 4.10: Wave form of an acoustic pulse 180 degrees out of phase from the pulse shown in figure 4.9

In order to arrive at the harmonic data using pulse inversion, the two sets of data that are out of phase are literally added together. The resulting signal then goes through the imaging process described in Chapter 5.

Chapter 5

Image Display

The goal in this mechanical sector, B-mode ultrasound system is to manipulate the collection of 1-D signals such that the resulting 2-D image will show gray-scale bands in areas where there are physical boundaries in the medium. In order to get the desired image, the data must be processed. For each of the techniques (pulse inversion, high-pass filter, and fundamental), as the 256 vectors of data are read into a PC, they are stored into a 2048 x 256 matrix. Each point (x, y) in the matrix stores a number between 0 and 255 (Figure 5-1).

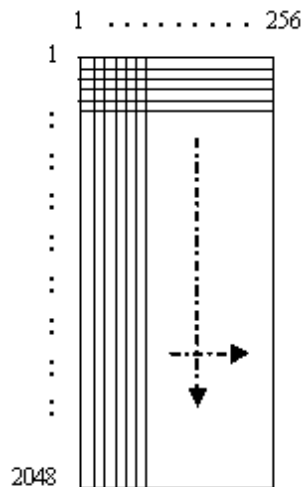


Figure 5.1: A 2048 x 256 collection of data

The remaining steps are all performed in Matlab. For pulse inversion, the two pulses of data are added. Then, for all three techniques, as described in the previous section, the saturated samples are removed and the data is windowed using a hanning window.

Next, for the high pass filtered harmonic data, the high pass filter is applied. Finally, for all three techniques, each of the vectors of data is rectified, then envelope detected. Once this is done to all 256 vectors of data, the matrix of modified data is scaled to a dynamic range of $[0, 255]$ and then forwarded to another algorithm for scan conversion and then image display.

5.1 Rectification

Rectification is the same as taking the absolute value of a signal. In software, this is achieved by replacing all the values with their absolute values. Figure 5.2 shows five periods of a sine wave before and after rectifying the sine wave.

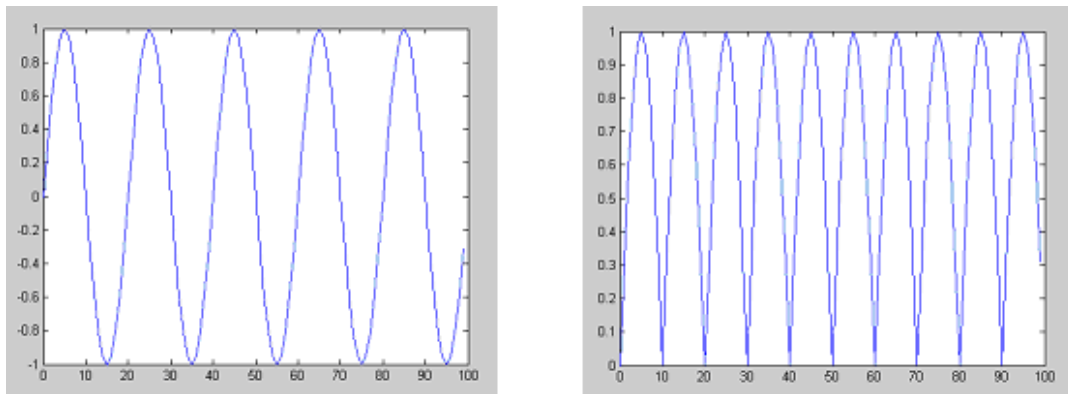


Figure 5.2: The first image shows five periods of a sine wave and the second image shows the signal after rectification

Looking at the above images, it is clear that rectification causes the introduction of higher frequency components. The magnitude of the DFT of both of the above signals are shown below in Figure 5.3.

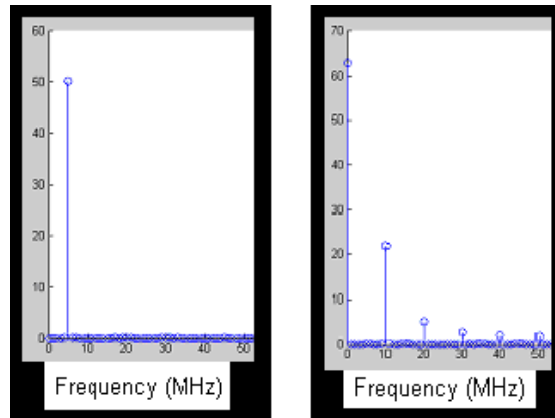


Figure 5.3: The first image shows the DFT for five periods of a sine wave and the second image shows the DFT for the five periods of a sine wave after rectification

In fact, rectification causes the fundamental frequency of the rectified signal to be two times that of its corresponding non-rectified signal. Additionally, harmonics of the new fundamental frequency get introduced into the frequency make-up of the rectified signal.

5.2 Envelope Detection

Envelope detection is performed to help with visualization of RF data on a computer display. A simplified example is used here to illustrate the concept of envelope detection. The data initially coming from a boundary from a single reflection is a wave that is similar, conceptually, to the wave shown in Figure 5.4. Rectification of the data introduces large jumps in gray scale values for adjacent samples. This is shown in Figure 5.5. Since, the goal is to see a gray-scale band in the image where a boundary exists, the goal of envelope detection is to adjust the data such that there is a smooth transition of gray scale values in a neighborhood of pixels. An example of an envelope for a single sine wave is denoted by the dotted line in Figure 5.6.

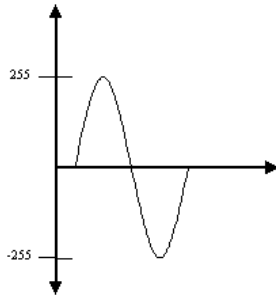


Figure 5.4: Original RF signal

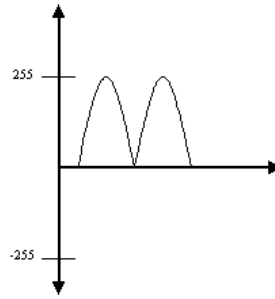


Figure 5.5: Rectified signal

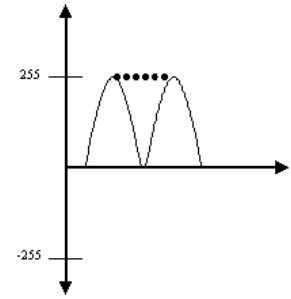


Figure 5.6: Dotted line shows the desired effects of envelope detection on the rectified signal

A mental exercise to visualize the desired effects of envelope detection for more complex signals is to imagine the shape of a blanket if it were dropped on top of a jagged signal, for example, the signal shown in Figure 5.7.

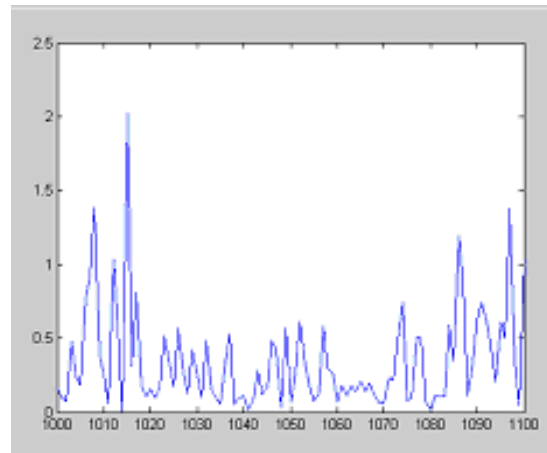


Figure 5.7: Ultrasound data

The transition from point to point in the signal should be smoothed so that the difference in gray scale values between neighboring values is reduced. A low pass filter performs this signal smoothing. The low pass filter can either be applied in the time domain using convolution or in the frequency domain using multiplication. Since the overall goal of this research is to build the system in hardware, the technique that can be done more easily in hardware is desirable. Since the data is already in the time domain, it is easier to perform convolution and therefore, avoid performing the DFT and the IDFT functions.

5.2.1 Averaging Envelope Detector

Initially, the averaging filter was employed as the envelope detector in this research. The function for this envelope detector is as follows. Each of the sample values in the vector was summed with the four sample values before it and then the total sum was divided by five. The corresponding filter shown graphically in Figure 5.8, slid over each vector of data with the fifth filter value starting at the first sample and ending at the fifth from the last sample. Along the way, the value which the fifth sample multiplied with was the sample that got replaced.

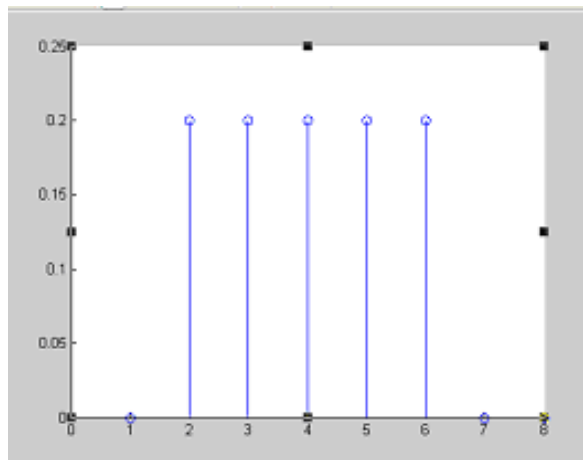


Figure 5.8: Averaging filter in spatial domain

This process is identical to convolution. Recall that a convolution performs the following using the functions $f(x)$ and $h(x)$:

1. Flip $h(x)$ about the origin.
2. Shift $h(x)$ over $f(x)$, having $h(x)$ start before $f(x)$ and finish after $f(x)$.
3. Each time $h(x)$ is shifted, the sum of the product of the overlapping values from the two functions is calculated and the resulting value replaces the sample value.

The averaging process is an example of performing convolution where the signal shown in Figure 5.8 is $h(x)$ and the vector of data is $f(x)$. This process is shown mathematically with the following equation:

$$y(x) = \sum_{u=0}^{M-1} h(u)f(x - u) \quad (5.1)$$

where $y(x)$ is the output sequence. Since performing convolution in the spatial domain is equivalent to performing multiplication in the frequency domain, this envelope detector is also a meaningful in its frequency domain representation. Figure 5.9 shows the magnitude of the DFT of $h(x)$.

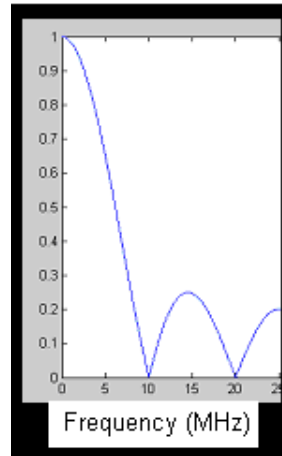


Figure 5.9: Magnitude of the DFT of the averaging filter

The envelope detector is intended to behave as a low-pass filter, and an ideal low pass filter is a rectangular function in the frequency domain [12]. Since the DFT of the averaging signal returns a function that only vaguely resembles a rectangular function in the frequency domain, a better envelope detector was created.

5.2.2 Optimized Envelope Detector

Since an ideal low pass filter, the desired envelope detector, is a rectangular function in the frequency domain, an envelope detector with a function that strongly resembles the ideal filter was created. First, a sinc function was created. This is because the inverse DFT of a rectangular function is an infinitely long sinc function. Since computers only can analyze finite length signals, the sinc function for the ideal low-pass filter inevitably must be truncated. This truncation many times is accomplished by setting all values outside of a portion of the continuous function to zero and leaving the remainder of the values untouched. This process is identical to multiplying a rectangular window with an infinitely long sinc function. Multiplying a rectangular window with the sinc function is a bad choice due to the large side lobes in the frequency domain representation of the rectangular window. These side lobes cause high frequencies to arise in the low pass filter. To limit the amount of high frequencies in

the low pass filter, a windowing function with minimized side lobes in its frequency domain representation was chosen. Although many windowing functions have minimized side lobes, in this research, a Hanning window was selected. Therefore, the resulting low pass filter used for envelope detection was a sinc function truncated using a Hanning Window. These functions are shown in Figure 5.10.

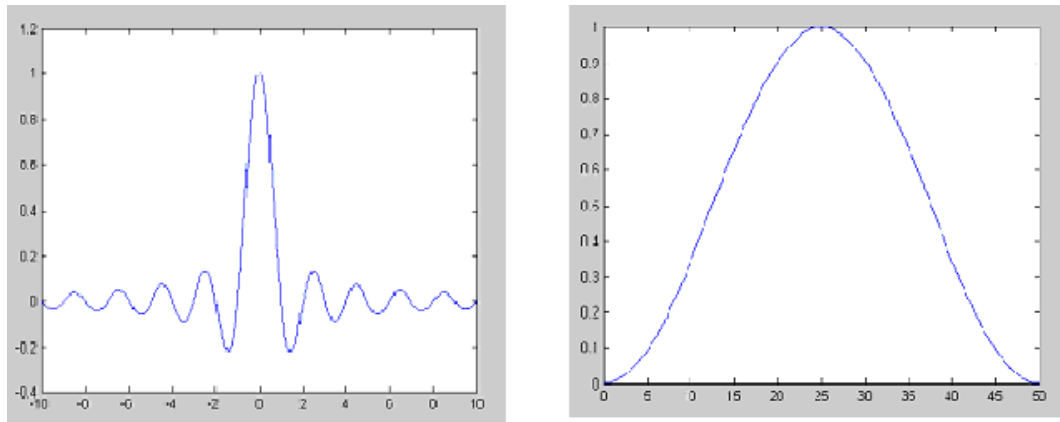


Figure 5.10: First image shows the sinc function and the second image shows the hanning window

In this research, two envelope detectors were created using this technique: a 31-tap filter for the fundamental data and a 27-tap filter for the harmonic data.

A graphical representation of the harmonic envelope detector in the time domain is shown in Figure 5.11. This filter was convolved with each vector of the harmonic data. Notice from the magnitude plot of the Fourier transform for this filter, the filter has a passband of approximately 3.24 MHz and almost no side lobes.

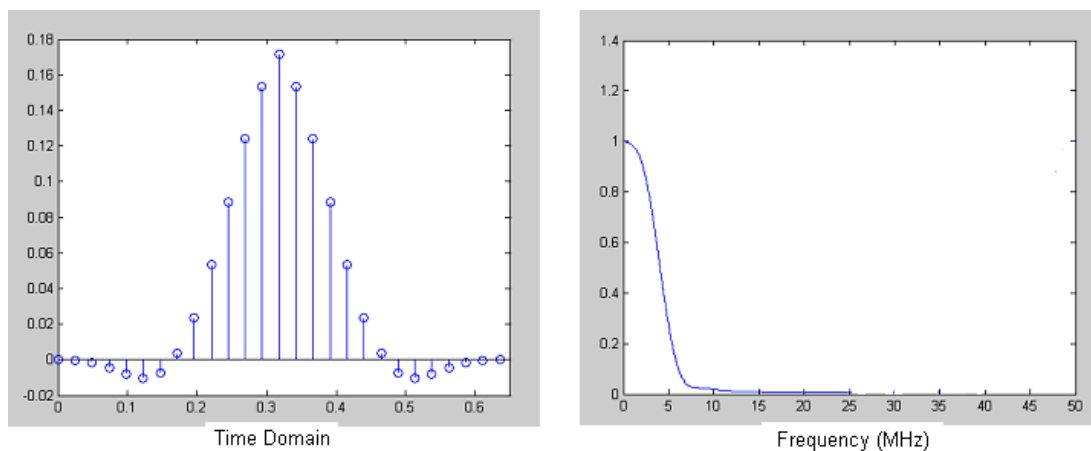


Figure 5.11: First image shows the harmonic enveloping detector the second image shows the DFT of the signal

Because a 3.5 MHz pulse frequency is used in this research, the second harmonic is at 7 MHz, and so the rectified data for the harmonic data is 14 MHz. As can be seen in Figure 5.11, this filter almost completely levels off to zero after 14 MHz. This is desirable for the harmonic frequencies which contain important information up to 14 MHz.

A graphical representation of the fundamental data envelope detector in the time domain is shown in Figure 5.12.

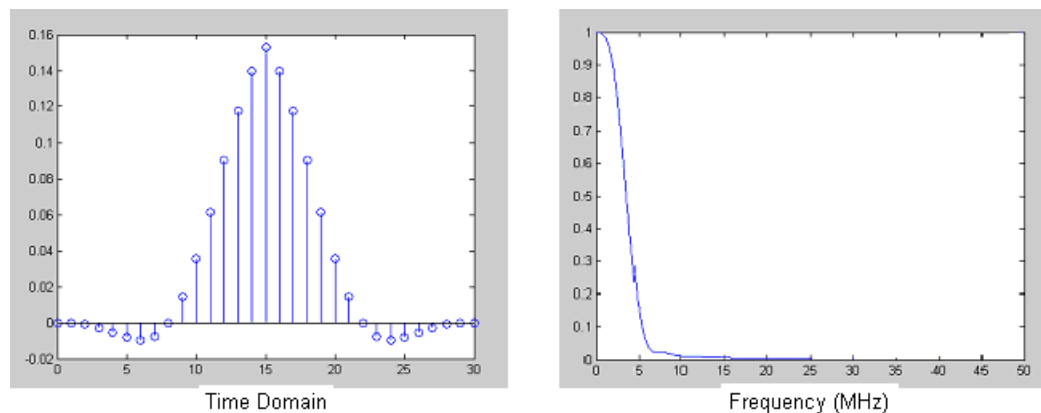


Figure 5.12: First image shows the fundamental enveloping detector the second image shows the DFT of the signal

Figure 5.12, it is seen that the 31-tap filter has a passband of 2.9 MHz and that the filter almost completely levels off at zero after 7 MHz. This is desirable for the

fundamental frequencies which only contain important information at frequencies as high as 7 MHz.

To summarize, envelope detectors were selected that most strongly resembled a low pass filter. Initially, an averaging filter was utilized. However, due to the large amount of higher frequencies contained in the averaging signal, a more optimal low pass filter was created using a sinc function and a Hanning window. Furthermore, in the optimized filter, more taps were taken in order to cause the cut-off frequency to be at a lower frequency.

5.3 Scan Conversion

Once data processing is complete, scan conversion is performed. Scan conversion converts the collected ultrasound data (which is in polar coordinates) into Cartesian coordinates. The technique utilized in this research comes from a paper titled Real-Time Ultrasonic Scan Conversion Via Linear Interpolation of Oversampled Vectors, by William D. Richard and R. Martin Arthur [9].

To summarize, the final image used to display the ultrasound data is composed of 512 x 512 pixels (Figure 5.13). The objective is to fit the data from the 256 x 2048 matrix into the image. Furthermore, the final image needs to be in Cartesian form, as shown in Figure 5.14.

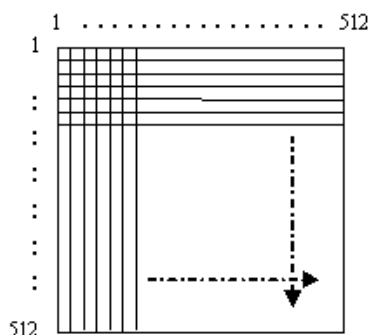


Figure 5.13: A 512 x 512 matrix of pixel values used to display the ultrasound data



Figure 5.14: A 512 x 512 image where the white portion denotes areas where sample data is inserted

The algorithm checks every pixel in the 512 x 512 image to determine if the point is within 45 degrees of the center axis and within a radius of 512 pixels from the pixel location (1, 256.5) (this area is the white region displayed in figure 5.14)¹. Pixels external to this region are set to be black, which is a grayscale value of zero. For every pixel located within the white region, a point from the image data is found to insert into that pixel location. Looking at Figure 5.15, the challenge in determining what sample to use is exemplified.

¹The hole at the top of the white region results from the fact that the transducer head moves as it collects each vector of data (pivot-to-face distance).

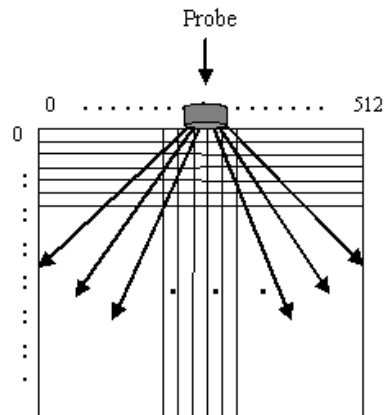


Figure 5.15: Overlap of the vectors from collected data introduces a challenge in determining what value should be displayed at a pixel location

It is possible that several or none of the vectors of data contain a sample value within a single pixel square. The method used to determine which vector to select the sample from is based on the mathematical equation supplied by the manufacturers of the GP2000 probe. The pixel location is input to an equation which returns an angle measure. Ideally, there would be a vector of data that would have been measured at that angle. However, because there may not be a vector of data at that precise angle, the nearest vector is chosen. An example is shown in Figure 5.16 where the dotted line shows the measured angle calculated by the sinusoidal equation. The nearest vector, B, is the vector that would be chosen by the algorithm.

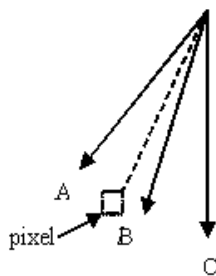


Figure 5.16: A pictorial example showing the method used to select a vector for sampling

Then, the sample value from the selected vector is chosen. Since the image is 512 pixels long while the vector sample contains 2048 points, there is a relationship of 1 pixel to every 4 samples. Therefore, the sample chosen is the sample that has an index value into the vector equal to four times the radius of the pixel location in the image.

As mentioned, this method of scan conversion is an example of nearest neighbor-interpolation. Although this method is sufficient for displaying images, there are other methods that perform better. For example, in the case of oversampling, it has been shown that both bilinear interpolation and linear interpolation with oversampling provide improved results [9].

5.3.1 Image Display

Once the algorithm finishes filling in the 512 x 512 image with grayscale values ranging from 0 to 255, the image is displayed such that each pixel in the image displays the gray scale value assigned to it.

Chapter 6

Results

In this section, images from a B-mode, mechanical sector system are shown.

6.1 Comparison of Envelope Detectors

Initially, an averaging filter was used to perform envelope detection. Then, an improved envelope detector for both fundamental and harmonic data was generated by utilizing the sinc function and a Hanning window.

Figure 6.1 shows the results of using the averaging filter envelope detector and the optimized envelope detector on the same set of fundamental data.

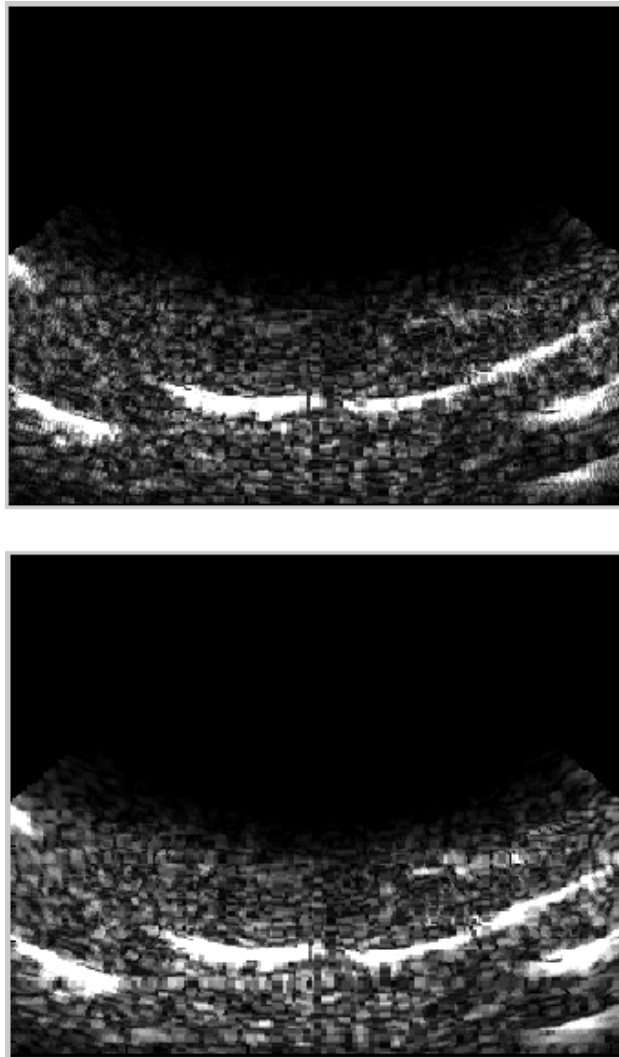


Figure 6.1: Two fundamental images: the first utilized an averaging envelope detector and the second utilized an optimized envelope detector

As seen in the images above, using the optimized envelope detector results in smoother transitions in gray-scale values.

Below, in Figure 6.2, are two images of the same harmonic data that result by applying the averaging filter and the optimized envelope detector.

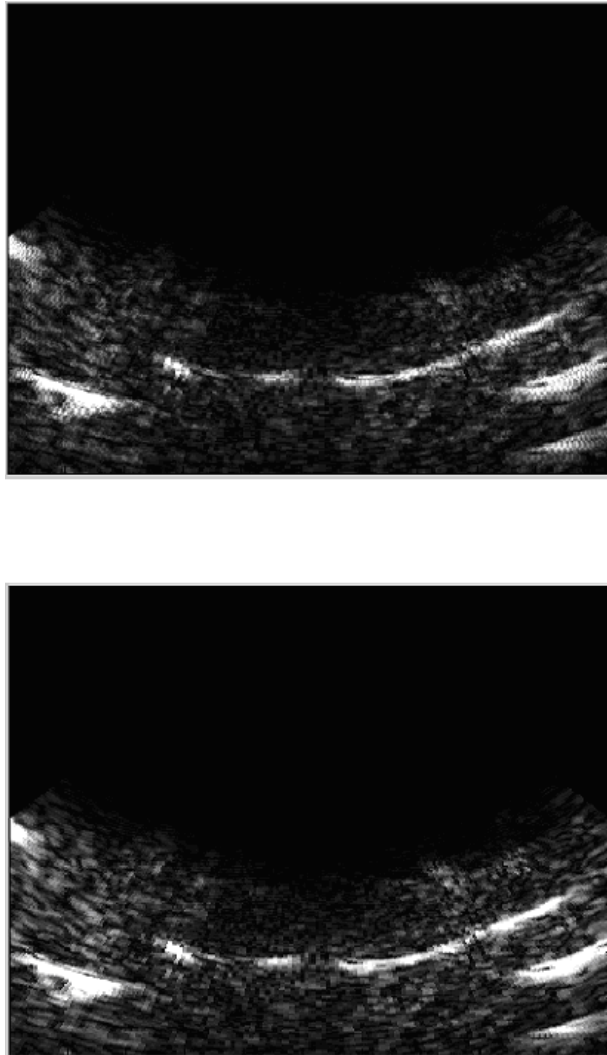


Figure 6.2: Pulse inversion harmonic images: the first utilized an averaging envelope detector and the second utilized an optimized envelope detector

The optimized envelope detector returns data with less artifacts quantitatively. Pictorially, as seen in Figure 6.2, the checkered appearance in the images in which the averaging envelope detector was applied is not seen in the images in which the optimized envelope detector was applied.

In all images that follow, the optimized envelope detectors were employed.

6.2 Fundamental vs. Harmonic Images

In the figures that follow, the two data files used for pulse inversion are shown in their fundamental form and then in their high-pass filtered harmonic form. Then, the fifth image shows the harmonic image derived from using pulse inversion.

An image of a cyst inside of a tissue mimicking phantom is shown in Figure 6.3.

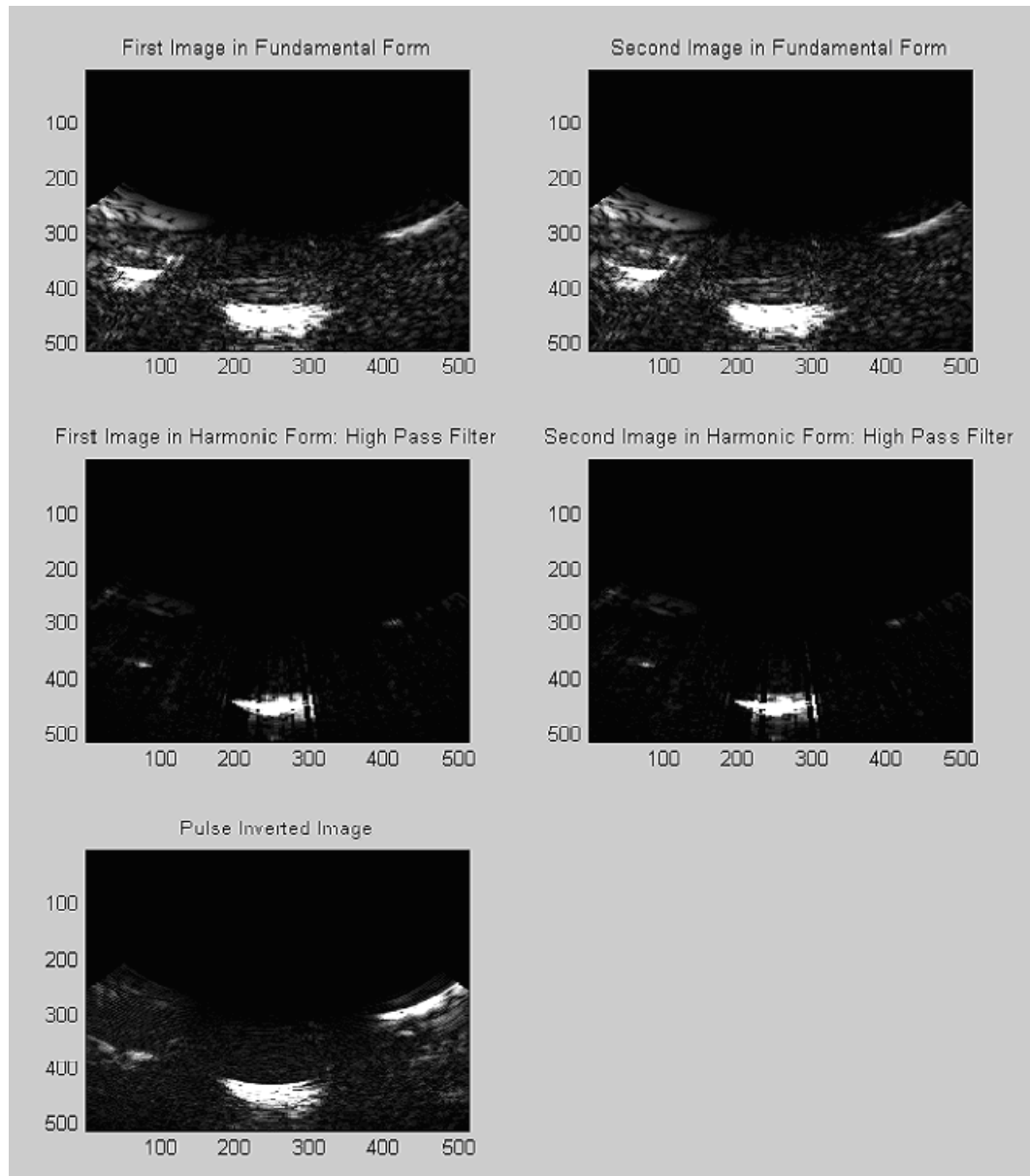


Figure 6.3: Fundamental and harmonic images of a cyst

An image of tissue in a tissue mimicking phantom is shown in Figure 6.4.

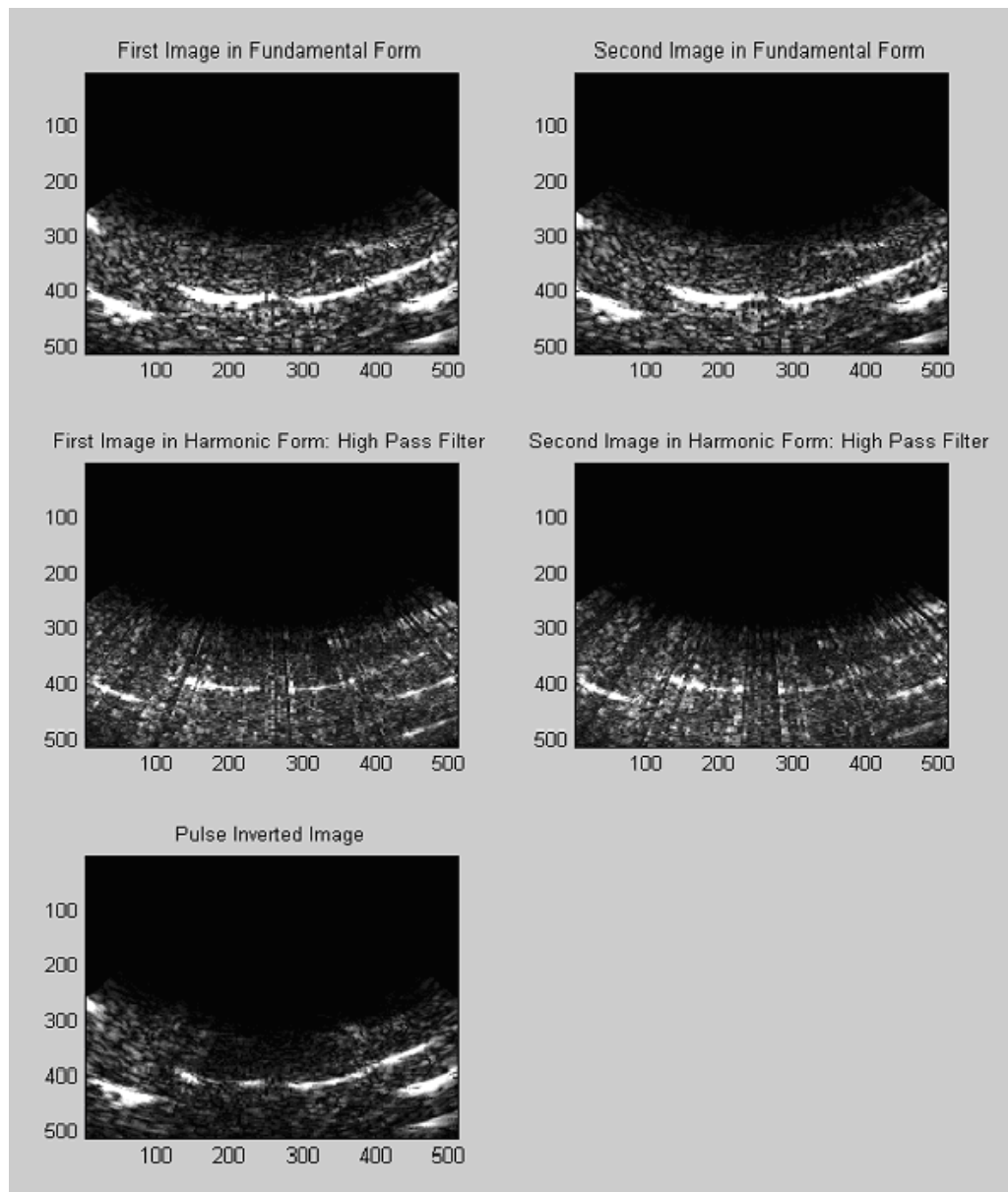


Figure 6.4: Fundamental and harmonic images of tissue-mimicking substance

The success of harmonic imaging with a B-mode, mechanical sector ultrasound system is illustrated in these images. Enough harmonic data was captured in the reflected signal to generate images. Furthermore, these images contain less noise than the fundamental images and have improved axial and lateral resolution.

6.3 Future Work

The next step is to make optimizations to the ultrasound system. An undesirable effect seen in the high-pass filtered images are ray-like lines running almost vertically throughout the images.

One possible cause of the undesirable effects in the high-pass filtered harmonic images could be the large amount of overlap of the fundamental and the first harmonic signal. Currently, the ultrasound system emits a single cycle of an ultrasound wave which causes the fundamental and harmonic bands to overlap. As a result, the filter inevitably removes some of the harmonic signal while keeping some of the fundamental signal. Altering the shape of the emitted ultrasound wave pulse so that the fundamental and harmonic signals do not overlap can be accomplished by emitting more cycles of the ultrasound wave. Such an alteration in sound wave shape would preserve the frequency content of the data, but would diminish the axial resolution in the images.

Another cause of the undesirable effects in the high-pass filtered harmonic images could be due to a poor choice of a high-pass filter. The importance of the choice of the high-pass filter can be seen in Figure 6.5.

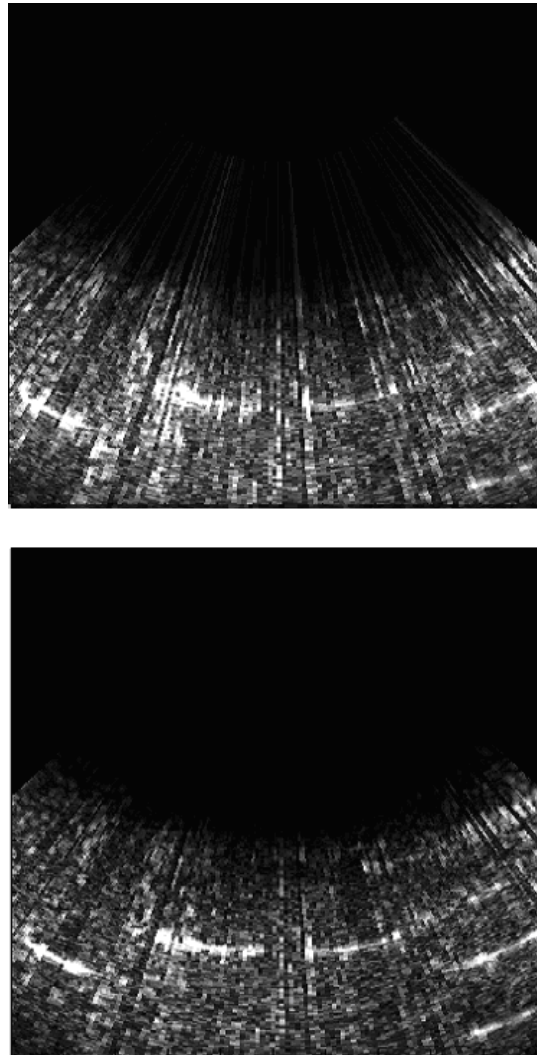


Figure 6.5: First plot shows an image obtained where an ideal filter is applied to the data and the second plot shows an image obtained where a Butterworth filter of order 8 is applied to the data

The two images were generated from the same set of data. The two images differ in that the first image was generated using an ideal high-pass filter while the second image was generated using a Butterworth high pass filter of order 8 with cut off frequency equal to 1.5 times the fundamental frequency. Figure 6.6, shows the two filters that were employed.

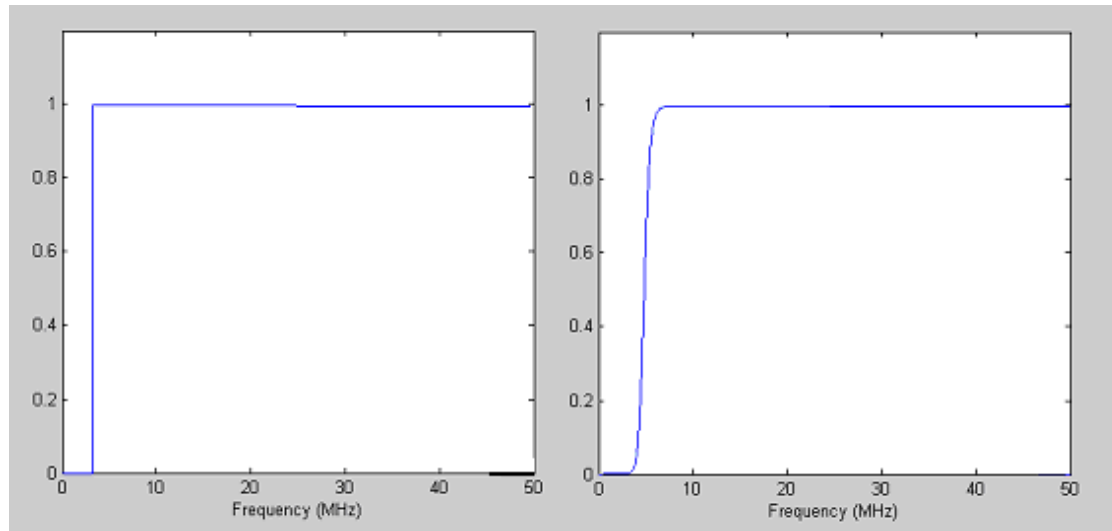


Figure 6.6: First plot shows an ideal filter and the second plot shows a Butterworth filter of order 8

It is clear that using the Butterworth filter diminished the ray-like effect that arises when using the ideal filter. It is possible that using a different filter may remove the ray-like effect even more.

To summarize, future work could be devoted to improving the high-pass filtered harmonic images by doing the following: alter the number of ultrasound waves emitted from the probe to reduce fundamental and harmonic frequency overlap and test more high-pass filters to find an optimal high-pass filter.

Chapter 7

Conclusions

Harmonic generation results from the physics of sound waves and their interactions with the media through which they travel. As sound waves propagate through a medium, they compress and expand the medium. Sound waves travel at a faster speed in compressed regions than in expanded regions. Consequently, as an ultrasound wave propagates through a medium, the shape of the sinusoidal wave that was initially pulsed into the medium transforms. This transformation indicates that there is an introduction of harmonic information into the propagating ultrasound wave.

The work presented in this paper demonstrates that this harmonic data can be utilized to generate harmonic images with a mechanical sector, B-mode ultrasound system. Furthermore, as predicted, objects in the images show higher resolution and less noise. The work presented so far is a preliminary step for implementing this system in real-time in hardware. It is worth noting that the system used for the testing above is not of optimal quality. Because harmonic images were able to be generated using a non-optimal system, the results indicate that future work into a real-time harmonic imaging system is not only possible, but may also be worthwhile.

Appendix A

Fourier Transform

Signals can be observed in both the spatial domain and the frequency domain. Signals in the frequency domain are expressed as a summation of sine and cosine functions at a multitude of frequencies (Fourier series). The key idea is that by adding together the sine and cosine functions specified from the frequency domain, the resultant function ends up being identical to the signal in the time domain. The Fourier transform is used to determine the frequencies making up a spatial domain signal while the inverse Fourier transform returns a signal in the frequency domain to the spatial domain representation. These two functions are called the Fourier transform pair. The transformation between these two domains results in no loss of information.

The research presented in this paper uses a 1-D discrete Fourier transform (DFT). DFT is a Fourier series representation of a discrete, finite length signal. This representation is desirable because a computationally fast algorithm, the Fast Fourier Transform (FFT), can evaluate DFTs on a digital computer or for implementation in digital hardware very quickly [6]. The equation for the DFT is as follows:

$$F(u) = \frac{1}{M} \sum_{x=0}^{M-1} f(x) e^{-\frac{jux2\pi}{M}} \quad (\text{A.1})$$

where M is the total number of samples, u is the u th frequency, and $f(x)$ is the value of the x th sample. Looking at Eulers equation in equation A-2 the concept of finding a signals component frequencies becomes clearer.

$$e^{j\theta} = \cos \theta + j \sin \theta \quad (\text{A.2})$$

The exponential in the DFT equation decomposes into a cosine and sine component and so the DFT actually evaluates frequency components.

The number of samples in the time domain equals the number of samples in the frequency domain. Consequently, the frequency for each sample in the frequency domain can be determined. For example, with a 50 MHz sampling rate, if 8 samples are taken, the frequencies in the Fourier transform are multiples of 6.25 MHz up to 50 MHz. However, with a 50 MHz sampling rate, if 256 samples are taken, the frequencies in the Fourier transform are all multiples of 195 kHz. The following equation can be used to determine frequency interval between two successive data points in the transform:

$$frequencyinterval = \frac{samplingfrequency}{numberofsamples} \quad (A.3)$$

Therefore, the frequency at the u th tick mark in the frequency domain would be u times the frequency interval.

As seen from equation A-2, performing the transform on a signal returns two values: a real value and an imaginary value. The following equation shows what is expected from the transform more generically:

$$z = x + j \times y \quad (A.4)$$

where x represents the real component, j is equal to $\sqrt{-1}$, and y represents the imaginary component. The magnitude of the frequency is determined using the following equation:

$$|F(u)| = \sqrt{x^2 + y^2} \quad (A.5)$$

The phase shift for each frequency is determined using the following equation:

$$\phi(u) = \tan^{-1} \left[\frac{y}{x} \right] \quad (A.6)$$

The resulting magnitude plot from a transform always is centered around $u = 0$ such that the functions to the left and right of the y-axis mirror each other over the y-axis. Both the positive and negative values have identical real values with the difference between the frequency values lying in the phase shifted portion. Filtering out a

particular frequency requires filtering out both the positive and negative portion in the transform.

The Matlab program represents DFTs slightly differently. The transform ranging from the leftmost position all the way to the y-axis is cut and pasted to the end of the positive portion of the transform. So the frequency value needs to be removed from both the positive transform and the pasted negative portion in order to filter out a particular frequency, both of which will be lying in the positive x-axis.

The inverse discrete Fourier transform is represented by the following equation:

$$f(x) = \frac{1}{M} \sum_{u=0}^{M-1} F(u) e^{\frac{jux2\pi}{M}} \quad (\text{A.7})$$

This equation is used to return the frequency domain signal back to the spatial domain.

Appendix B

DFT Leakage and Windowing Functions

When a continuous signal that is periodic by nature is sampled, the signal may still appear non-periodic in the transform; this is because the sampling did not capture an exact integer number of cycles of the period [9]. This is exemplified pictorially in figures B.1-B.3.



Figure B.1: A continuous periodic signal

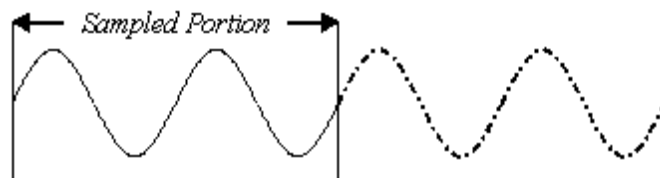


Figure B.2: Sampling exactly 2 samples of the continuous periodic signal and replicating this sampled signal into a periodic signal

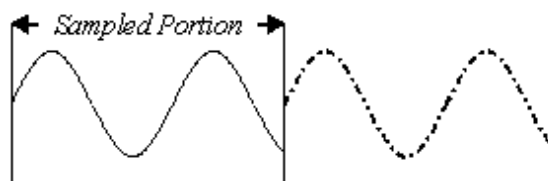


Figure B.3: Sampling a non-integer amount of periodic sample and replicating this sampled signal into a periodic signal. Discontinuities arise

From figures B.1-B.3, it is clear that if the starting and stopping values of the signal do not meet up in a continuous manner, when the sampled data is replicated into a periodic signal, a discontinuity arises. Because the sampled signal in figure B.2, when replicated, does not contain any discontinuities, the DFT results in only a single spike at the frequency of the signal. On the contrary, the sampled signal in figure B.3 does not capture the periodic nature of the naturally periodic signal. In order to represent the signal in the DFT, the discontinuity must be represented by higher frequencies. Therefore, the DFT for figure B.3 contains higher frequencies simply because a non-integer number of cycles were sampled. This introduction of artificial frequencies is called *leakage*.

The standard method of sampling data from a continuous time signal is an example of multiplying a rectangular window with a width of the sample interval against the continuous time signal [Figure B.4]. All values outside the sampled interval are set to zero while all values within the sampled interval are multiplied by one.

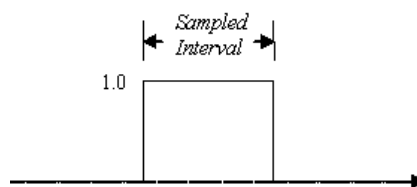


Figure B.4: Rectangular window

This is important to note, because rectangular windows introduce a great amount of leakage. The DFT of the rectangular function is the sinc function ($\sin(x)/x$), and a plot of the sinc function shows that there are many side lobes with large magnitudes with respect to the main lobe. These side lobes cause the DFT leakages. Therefore, in order to minimize the leakage, it is necessary to reduce the side lobe amplitudes.

This is achieved by using windowing functions other than the rectangular function to collect the sampled data [12].

Three indicators for determining the effectiveness of a window can be determined by the frequency domain representation of a window. These indicators are [12] :

- Peak side lobe magnitude with respect to the main lobe magnitude
- Speed at which the side lobes decrease as the frequency increases
- The width of the main lobe

Windowing functions are a tradeoff between these three criteria, which are shown pictorially in figure B.5.

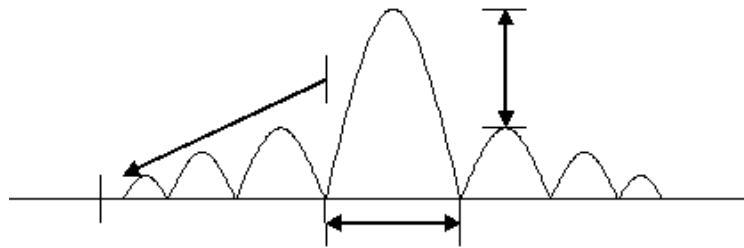


Figure B.5: An example of a frequency domain for a windowing function

An extensive analysis and comparison of windowing functions is found in Harris article, “On the Use of Windows for Harmonic Analysis with the Discrete Fourier Transform” [9]. From his work, it is shown that each window has unique strengths and weaknesses. The choice of a window function depends on the requirements for the windowing function by the application in which it is used [9].

References

- [1] Bouakaz, Ayache, Egon Merks, Charles Lancee, and Nicolaas Bom. 2004. Non-invasive Bladder Volume Measurements Based on Nonlinear Wave Distortion. *Ultrasound in Medicine & Biology* 30:469-476.
- [2] Duck, Francis A. 2001. Nonlinear Acoustics in Diagnostic Ultrasound. *Ultrasound in Medicine & Biology* 28:1-18.
- [3] Duck, Francis A. 1990. *Physical Properties of Tissue: A comprehensive Reference Book*. London: Academic Press. 28:1-18.
- [4] A.P. Cracknell. 1980. *Ultrasonics*. Great Britain: Wykeham Publication (London) Ltd.
- [5] Frinking, Peter J. A., Ayache Bouakaz, Johan Kirkhorn, Folkert J. Ten Cate, and Nico de Jong. 2000. Ultrasound Contrast Imaging: Current and New Potential Methods. *Ultrasound in Medicine & Biology* 29:965-975.
- [6] Precision Small Parts Grey Scale Phantom. *Gammex*. <https://www.gammex.com/catalog/> (Accessed 8 July, 2005).
- [7] Haerten, R., C. Lowery, G. Becker, M. Gebel, S. Rosenthal, and E. Sauerbrei. 1999. EnsembleTM Tissue Harmonic Imaging: The Technology and Clinical Utility. *Electromedica* 1:50-56.
- [8] Hamilton, Mark F. and David T. Blackstock, eds. 1998. *Nonlinear Acoustics*. San Diego: Academic Press.
- [9] Harris, F. 1978. On the Use of Windows for Harmonic Analysis with the Discrete Fourier Transform. *Proceedings of the IEEE*. 66: 51-83.
- [10] Hsu, Hwei P. 1995. *Signals and Systems*. New York: McGraw-Hill.

- [11] Lempriere, Brian M. 2002. *Ultrasound and Elastic Waves*. New York: Academic Press.
- [12] Lyons, Richard G. 2004. *Understanding Digital Signal Processing*. New Jersey: Prentice Hall.
- [13] Macovski, Albert. 1983. *Medical Imaging*. London: Prentice-Hall International, Inc.
- [14] Pierce, Allan D. 1981. *Acoustics*. New York: McGraw-Hill Book Company.
- [15] Radiated Fields of Ultrasonic Transducers. *NDT Resource Center*. <http://www.ndt-ed.org/EducationResources/CommunityCollege/Ultrasonics/EquipmentTrans/radiatedfields.htm> (Accessed 8 July, 2005).
- [16] Richard, William D., Martin Arthur. 1994. Real-time Ultrasonic Scan Conversion Via Linear Interpolation of Oversampled Vectors. *Ultrasonic Imaging*. 16:109-123.
- [17] Rossing, Thomas D. 1982. *The Science of Sound*. Reading: Addison Wesley Publishing Company, Inc.
- [18] Rumack, Carol M., Stephanie R. Wilson, J. William Charboneau, and Jo-Ann M. Johnson. 2005. *Proceedings of the IEEE*. China: Elsevier Mosby.
- [19] Stephens, R. W. B., and A. E. Bate. 1966. *Acoustics and Vibrational Physics*. Great Britain: William Clowes and Sons.

Vita

Danna Gurari

Date of Birth July 5, 1982

Place of Birth Buffalo, New York

Degrees B.S. Cum Laude, Biomedical Engineering, May 2005

August 2005